Review

Current Trends in Photonic Biosensors: Advances towards Multiplexed Integration

Jhonattan C. Ramirez [1,†], Daniel Grajales García [2,†], Jesús Maldonado [3,*] and Adrián Fernández-Gavela [4,*]

1 Departamento de Engenharia Eletrônica, Universidade Federal de Minas Gerais (UFMG), Belo Horizonte 31270-901, Brazil
2 School of Engineering and Sciences, Tecnológico de Monterrey, Monterrey 64849, Mexico
3 Department of Neurosurgery, School of Medicine, Yale University, New Haven, CT 06510, USA
4 Physics Department, University of Oviedo, 33007 Oviedo, Spain
* Correspondence: jesus.maldonadovazquez@yale.edu (J.M.); fernandezadrian@uniovi.es (A.F.-G.)
† These authors contributed equally to this work.

Abstract: In this review, we present the current trends in photonic biosensors, focusing on devices based on lab-on-a-chip (LOC) systems capable of simultaneously detecting multiple real-life diseases on a single platform. The first section lists the advantages and challenges of building LOC platforms based on integrated optics. Some of the most popular materials for the fabrication of microfluidic cells are also shown. Then, a review of the latest developments in biosensors using the evanescent wave detection principle is provided; this includes interferometric biosensors, ring resonators, and photonic crystals, including a brief description of commercial solutions, if available. Then, a review of the latest advances in surface plasmon resonance (SPR) biosensors is presented, including localized-SPRs (LSPRs). A brief comparison between the benefits and required improvements on each kind of biosensor is discussed at the end of each section. Finally, prospects in the field of LOC biosensors based on integrated optics are glimpsed.

Keywords: photonic biosensor; multiplexed detection; LOC; real-life applications; solutions

1. Introduction

Biosensors are self-contained integrated devices capable of transforming biomolecular binding events between a biomarker of interest and bioreceptor into quantitative or semi-quantitative analytical information useful to the user, achieved through spatial contact with a transduction element. This involves a biochemical receptor and a transducer to convert the binding event into electrical signals for further processing into information. Hence, biosensors can be classified based on their transduction principles as electrochemical, optical, and mechanical; or based on their biorecognition element as immunochemical, non-enzymatic, enzymatic, whole-cell, or DNA [1].

The first and most emblematic biosensor is the electrochemical glucose monitor developed in the 1970s. Since then, thanks to the advances in nanotechnology, biotechnology, and information technologies, several applications of biosensors have been commercialized to detect pregnancy hormones, cancer biomarkers, SARS-CoV-2 and antigens, rare genetic diseases, pollutants in soil or water, industrial food processes, and other biomarkers of interest to the public. However, there are still challenges in the process of bringing more applications out of the research laboratories to the mass population, and the list of biological elements to detect just keeps growing.

The main fields of applications of biosensors are industries where the detection of biological elements is critical, such as clinical human health (military, diagnostics, and monitoring), agro-industrial (veterinary, crops, and food production), and finally, environmental applications (soils, water, air). One of the key requirements for the detection of biological elements in any of these fields is the simultaneous detection (i.e., multiplexing) of

different biomarkers with the aim of obtaining a more reliable diagnosis. Moreover, a direct and simple readout is desirable, so the final user does not need to perform complicated tasks. Ideally, biosensors should be portable, with high sensitivity, label-free detections, and low fabrication costs. Additionally, it should be possible to integrate all the functionalities necessary to perform biological detections in a single device known as a lab-on-a-chip (LOC) platform [2]. These platforms include all the microfluidics necessary to deliver the sample of interest to the surface of the biosensor. One of the most popular materials for the fabrication of microfluidic cells is polydimethylsiloxane (PDMS) due to its transparency, easiness of fabrication methods, integration with valves and pumps, and the possibility of usage in several bioanalytical tests. Some of the newer materials employed are cyclo-olefin copolymers (COC) or perfluoropolyether (PFPE), offering low fabrication costs and light weight. Thermoplastics such as polymethyl methacrylate (PMMA) or polycarbonate (PC) are frequently used due to their mechanical stability, transparency, and low thermal conductivity. Newer materials such as COP or COC have been employed thanks to their optical properties. Paper can also be employed to build microchannels or surface patterns, normally after a hydrophobic or hydrophilic surface treatment designing the desired patterns [3]. For example, Klapperich et al. have developed a progesterone paper-based sensor using fluorescence of DNA strains with fluorescent IR dyes on the tip of them [4], and the detection of Escherichia coli was developed by Merkoçi et al. [5]. Some of the remaining challenges are the sealing and alignment between the microfluidic cell and the biosensor [6].

Thus, there is a growing demand for biosensors that provide the conditions for the simultaneous detection of multiple diseases on a single platform [7–10], preferably using non-invasive analytical processes [7] and avoiding the use of complex reagents (i.e., label-free). Traditional biosensors present difficulties in being integrated into devices with optimal performance and simultaneously meeting the requirements previously described. Biosensors like amperometric [7,11], colorimetric [8], and enzyme-linked immunosorbent assay (ELISA) [9] have shown excellent performance over the years, and even today, these technologies are used to develop commercial equipment, incorporating direct readout mechanisms, and multiplexing capabilities, if required.

On the other hand, integrated photonic biosensors offer advantages since their fabrication can be collectively performed, and multiplexing is relatively simple. Thus, the use of integrated optical biosensors has significantly increased in recent years due to their low production cost, high sensitivity, shielding to electromagnetic noise, real-time and label-free detection, easy interpretation of the measured data, and their ability to guarantee excellent biofunctionalization processes on the surface. However, due to the complexity of integration, optical-based technologies have slowly gained the expected acceptance [2]. Integrated photonics allows the creation of multiplexed biosensors within LOC platforms, where interferometers [12], resonant cavities [13], photonic crystals [14], and integrated plasmonic devices [15] have demonstrated excellent performance.

This review presents the last advances in multiplexed optical biosensors for the simultaneous and real-time detection of multiple pollutants, biomarkers, and diseases. Through studies conducted with new materials and optimized design and fabrication processes, it is possible to build highly sensitive and stable devices integrating all the required subsystems to perform the laboratory analysis on a chip.

2. Evanescent Waveguide-Based Biosensors

Most optical biosensors base their operating principle on the evanescent wave escaping a few nanometers on the surface of a waveguide where light propagates and its interaction with the external environment in the vicinity of the surface. Such interaction provides variations in the signal obtained at the output of the device, according to modifications on the exterior. Since the evanescent wave penetrates only a few nanometers, it is shielded from events occurring in the bulk of the sample, providing great sensitivity. Moreover, silicon surface biochemistry has been widely studied over decades providing reliable chemo

and biofunctionalization processes for the surface. Devices based on the evanescent wave interactions for chemical or biological detections have been studied with interest for their potential for integration, multiplexing, and improvement of sensitivity, with the aim to obtain POC diagnostics systems with LOCs.

2.1. Interferometric Biosensors

The working principle of an interferometric device consists of the superposition of two waves. Depending on the phase difference between the two waves, a signal with a specific intensity will result. If a modification is made in one of the two waves, there will be a variation in the intensity or in the phase of the resulting signal, which can be quantified. The shift of the interferometric pattern will be directly related to the variation produced in one of the waves. For optical biosensors, one of the waves is used as a reference, and the other one is in contact with the analyte; hence the interferometric signal will be directly proportional to the modification made in the arm, which interacts with the analyte.

Interferometric sensors constitute the most sensitive method for biosensing applications, and there are many different configurations to conduct this principle of operation [16–19]. In this subsection, we focus on devices based on waveguides since they are the ones with the greatest projection for their integration and multiplexed operations. Therefore, interferometric sensors based on integrated optics are one of the best candidates for POC devices shortly [20–23].

The first interferometer waveguide-based biosensing application was reported in the early 1990s [24]. This interferometer was based on the Mach-Zehnder interferometer (MZI), in which the light is separated into two different arms, and after a certain distance, both signals are recombined using a Y-junction, as Figure 1a shows. In 1994, the first Young interferometer (YI) was proposed [25]. The first application of YI as a biosensor was reported in 2000, reaching a bulk sensitivity of 9×10^{-8} RIU 26]. In YI, a Y-junction is used to divide one optical path into two arms. Unlike the MZI, the interference pattern is produced out-chip because there is no recombination of the two arms, as Figure 1b shows.
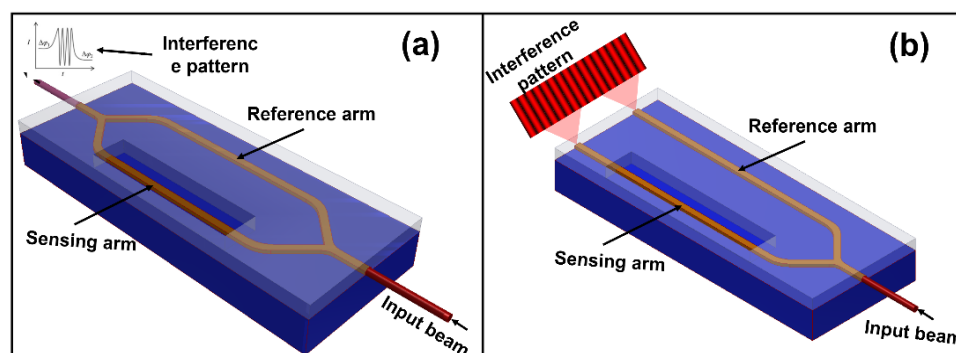

Figure 1. Interferometric biosensors. (**a**) Scheme of a standard Mach-Zehnder interferometer. The light is split into two arms and recombined at the output by on-chip Y-junctions. (**b**) Scheme of a standard Young interferometer. Rather than using Y-junctions to merge the split beams, the light is projected from two closely spaced secondary sources onto a display device.

Over the years, to improve the sensitivity, integration, and cost-efficiency of these sensors, new configurations have been developed by different research groups [26–31]. In recent years, the increase of people working in photonics has led to the advanced development of new high-performance interferometric devices. The integration of a ring resonator in one arm of an MZI could increase the sensitivity of the sensor 50 times [32]. This integration can increase the multiplexing capabilities of the sensor because the output signals in an MZI and ring resonator can be simultaneously obtained (see Figure 2a) [33]. As MZI sensors work using the evanescent field principle, the design of a waveguide with a high evanescent field can improve the sensitivity of the sensor, as demonstrated in 2021 [34]. However, the progress in the design of new structures has some limitations imposed

by the fabrication capabilities of the manufacturers. Another alternative to increase the sensitivity is by making some improvements in the measurement setup: the reduction of the mechanical and electric noise could reduce the sensitivity by two orders of magnitude (see Figure 2b). As Leuermann, J. et al. demonstrated reaching a bulk sensitivity of 1.4×10^{-8} RIU, the lowest reported in an MZI until today [35].

Although interferometric sensors are the most sensitive devices proposed, the difficulties that can be caused by the ambiguity in interferometric signals are a problem to overcome. To implement a modulation in the MZI without complex fabrication and bulk electronic equipment, an all-optical modulated MZI was implemented and applied in an immunoreaction of the hGH and anti-hGH pair [36]. In addition, coherently detected sensors were demonstrated as an attractive alternative to overcome the limitation of the quadrature point [37,38]. This coherent scheme was applied in an MZI with a low-cost laser source, obtaining a sub-nanogram per milliliter LOD in C-reactive protein immunoassays [39]. Another alternative for a low-cost interferometric modulation is the use of a broadband laser at the input of the waveguide. After all the wavelengths travel through the MZI, a spectral filter was integrated before the grating output. In this way, an output for each wavelength was obtained using different grating couplers, as Figure 2c shows [40]. The analysis of the shift in each wavelength using a CCD camera was applied for the detection of tuberculosis in human urine samples, reaching an LOD of 475 pg/ML using a direct immunoassay [41].
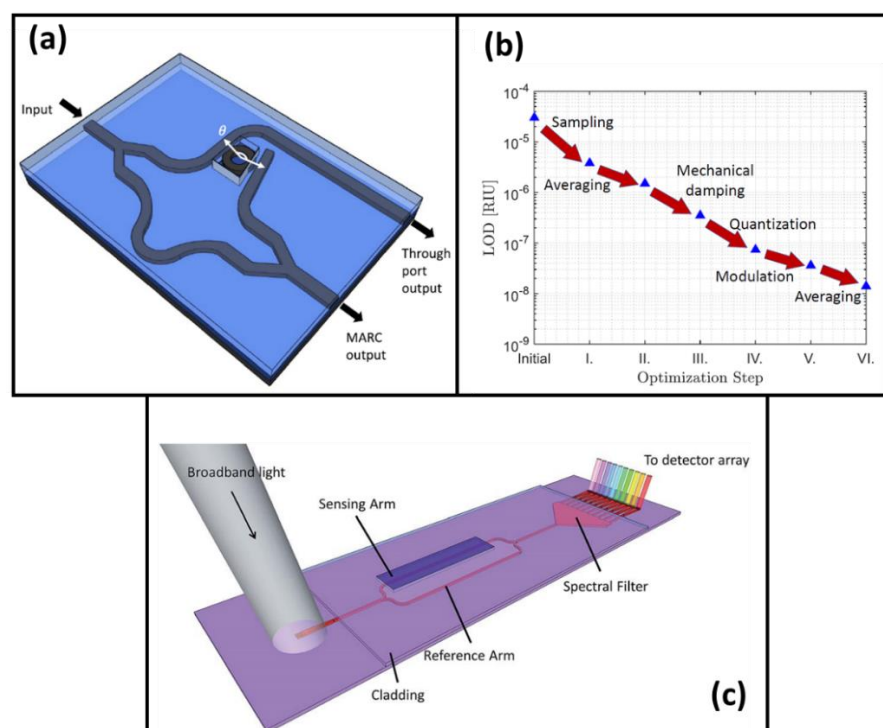

Figure 2. Improving sensitivity for interferometric sensors. (**a**) Scheme for the integration of a ring resonator in one arm of MZI. (**b**) Measured limit of detection of an integrated waveguide-based sensing system as different noise sources is addressed. (**c**) Scheme of an MZI sensor with an on-chip spectral filter integrated for linear readout. (**a**) Reprinted with permission from ref. [33], copyright 2022, The Optical Society; (**b**) reprinted with permission from ref [35], copyright 2019, MDPI; (**c**) reprinted with permission from ref [40], copyright 2018, the Royal Society of Chemistry.

More recently, a novel interferometer for biosensing applications was developed: the Bimodal Waveguide (BiMW) [42]. Compared with an MZI, on this device, the beam is not split into two different arms. The light excites two transversal modes with the same polarization on a common path. The interference between the two modes leads to a modal overlap, which will be modified if any perturbation is produced in the evanescent field

of the bimodal section. The sensitivity reached by the BiMW is in the range of the better interferometric sensors thus far reported, 5×10^{-8} RIU [43]. To get a linear readout with a BiMW, an all-optical modulation was implemented [44] in 2015. Recently, as an update of this modulation, adding a subsequent trigonometry-based algorithm has been proposed and applied for the selective identification and quantification of the external spike (S) protein of the severe acute respiratory syndrome coronavirus-2 (SARS-CoV-2) [45]. To improve the sensitivity or adapt to the current fabrication process for the mass production of common path interferometers, new configurations have been proposed: a bimodal interferometer with two lateral modes [46], trimodal waveguide (TriMW) [47], or a high-order multimode waveguide interferometer [48].

One of the greatest advantages offered by interferometric sensors is their integration and multiplexing capacities. At the beginning of the development of biosensing devices, most of the sensors were fabricated using the telecommunications structures in silicon, which needed expensive equipment because they work using the infrared wavelength range. Recently, the use of the SiN-on-silica platform opened the door to new structures which could operate in the visible range, which makes possible the implementation of low-cost POC devices with multiplexed capabilities [23,49]. In the last decade, the monolithic integration of label-free optical immunosensors was demonstrated [50]. Recently, a laser diode has been integrated into a silicon nitride MZI biosensor with a complete microfluidic cartridge to measure the concentration-dependent binding of streptavidin on a polyethyleneimine-biotin [51] (see Figure 3a). On the other hand, the necessity of microfluidic and flow delivery systems complicates the integration; to overcome that, a directly immersible MZI immunosensor has been developed, as Figure 3b shows [52]. The potential of this immersible sensor was demonstrated with the detection of antibodies against SARS-CoV-2 in human serum samples reaching an LOD of 20 ng/mL.

Regarding multiplexing capabilities, in the last five years, MZIs have been employed for many applications due to the easiness of in-out-couple the light using a fiber array unit (FAU). The use of a grating coupler and Y-junctions for on-chip beam splits led to the possibility of performing 4, 8, 16, 32, etc. measures at the same time, as Figure 3c,d show [53]. This kind of multiplexed integration has been used for aflatoxin M1 (AFM1) detection, reaching 16.8 pg/mL in purified and concentrated milk [54]. The detection of periostin (POSTN) and transforming growth factor beta-induced protein (TGFBI) is achieved in cancer patient serum with the use of these multiplexed MZIs [55]. Sensitive detection of anti-SARS-CoV-2 antibodies in human plasma that targets one or more viral antigens was demonstrated in [56]. Protein [57] or water pollutants [53] were detected using this multiplexed platform as well.

In addition to the applications previously mentioned for multiplexed devices, during 2022, MZIs have been used for the detection of acetone in the gaseous form, reaching an LOD of 0.76 ppm, making it feasible to be used for the diagnosis of diabetes and the prognosis of heart failure [58]. Also, simultaneous detection of *Salmonella typhimurium* and *Escherichia coli* O15:H7 in drinking water and milk was demonstrated in [59] with an LOD of 40 CFU/mL and 110 CFU/mL, respectively. Finally, we mention other biosensing applications carried out by BiMW, which prove the great capabilities of interferometric-based biosensors for the near future: monitoring of Irgarol 1051 [60] and fenitrothion [61] in water with an LOD of 3 ng/L and 0.29 ng/mL, respectively; detection of bacteria associated with nosocomial infection such as *Pseudomonas aeruginosa* and methicillin-resistant *Staphylococcus aureus* (MRSA), which achieved an LOD of 800 CFU/mL for both bacteria [62]; quantitative detection of *Bacillus cereus* in a buffer medium and *Escherichia coli* in undiluted ascitic fluid from cirrhotic patients, reaching an LOD of few bacteria per milliliter [63]; and the direct detection and quantification of miR-181a at attomolar concentrations (LOD = 23 aM) in human urine samples of bladder cancer patients with no need for prior sample purification or amplification steps [64].
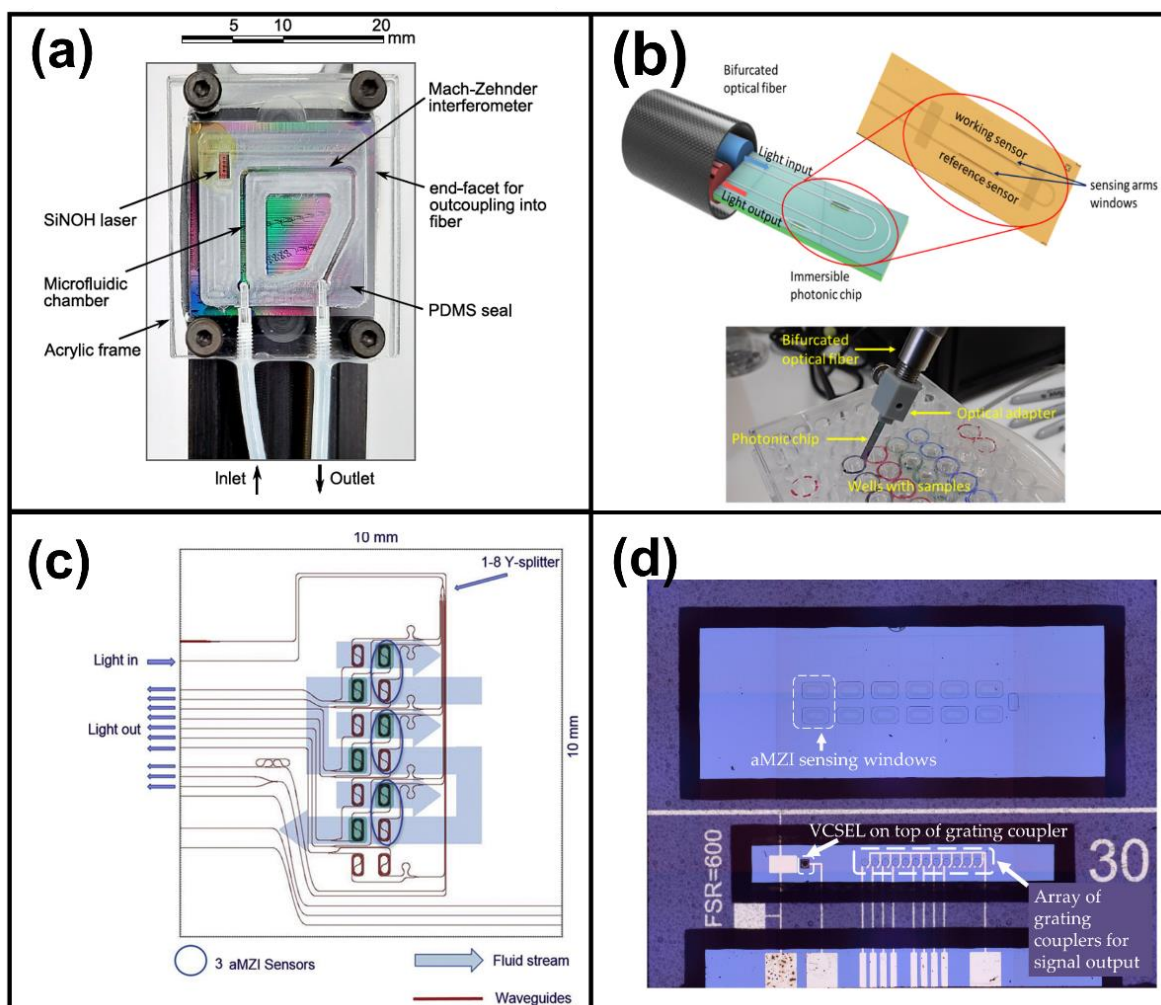
Figure 3. Integration of MZIs for multiplexed measures. (**a**) SiNOH laser integration in a photonic chip inside a microfluidic cartridge for biosensing applications. (**b**) Directly immersible MZI immunosensor without the need for a microfluidic cartridge and flow delivery system. (**c**) Overview of a multiplexed sensor, showing the full integration of light in- and out-coupling and the fluid stream for the measures of four MZIs at the same time. (**d**) Microscope photograph of MZI chip with hybrid integration of vertical-cavity surface-emitting laser (VCSEL) and photodiodes for multiplexed measures. (**a**) Reprinted with permission from ref. [51], copyright 2022, Elsevier; (**b**) reprinted with permission from ref. [52], copyright 2022, Elsevier; (**c**) reprinted with permission from ref. [53], copyright 2019, Elsevier; (**d**) reprinted with permission from [54], copyright 2019, MDPI.

2.2. Ring Resonator Biosensors

Photonic ring resonance refers to light being trapped in a resonant structure, continuously circulating, generating an evanescent field on the surface, and resulting in the removal of a specific wavelength among the ones contained in the light source (i.e., the resonance frequency ω) [65]. Thus, the presence of the analyte can be related to the resonance frequency shift $\Delta\omega$ caused by the increase in the diameter of the resonant structure because of the binding event on the surface of the assembly [66]. Several geometries have been developed through decades (see Figure 4): microspheres, domes, micro disks, toroidal shapes, and ovals or racetracks [67,68]. A novel geometry is the design of sub-wavelength structures to enhance the sensitivity of ring resonators using e-beam lithography on silicon-on-insulator for its fabrication [69]. A unique suggestion is the creation of a ring cavity by Kwon in 2017, where the ring resonator was etched as a plasmonic cavity in the substrate [70].

The most common fabrication methods are CMOS standard processes such as photolithography, and wet etching in silicon oxide, silicon nitride, or silicon-on-insulator

(SOI) [71]. Moreover, it is possible to acquire commercial designs from fabricants such as FBK8 or AIM photonics [72,73], among others. Further researchers have fabricated whispering gallery mode (WGM) resonators on the tip of fiber optics using home-built setups to melt the glass fiber into spheres with a CO_2 laser [74]. Sometimes gold nanoparticles or quantum dots (QD) can be integrated into the surface of the resonant structure to improve the limit of detection of the system [74].
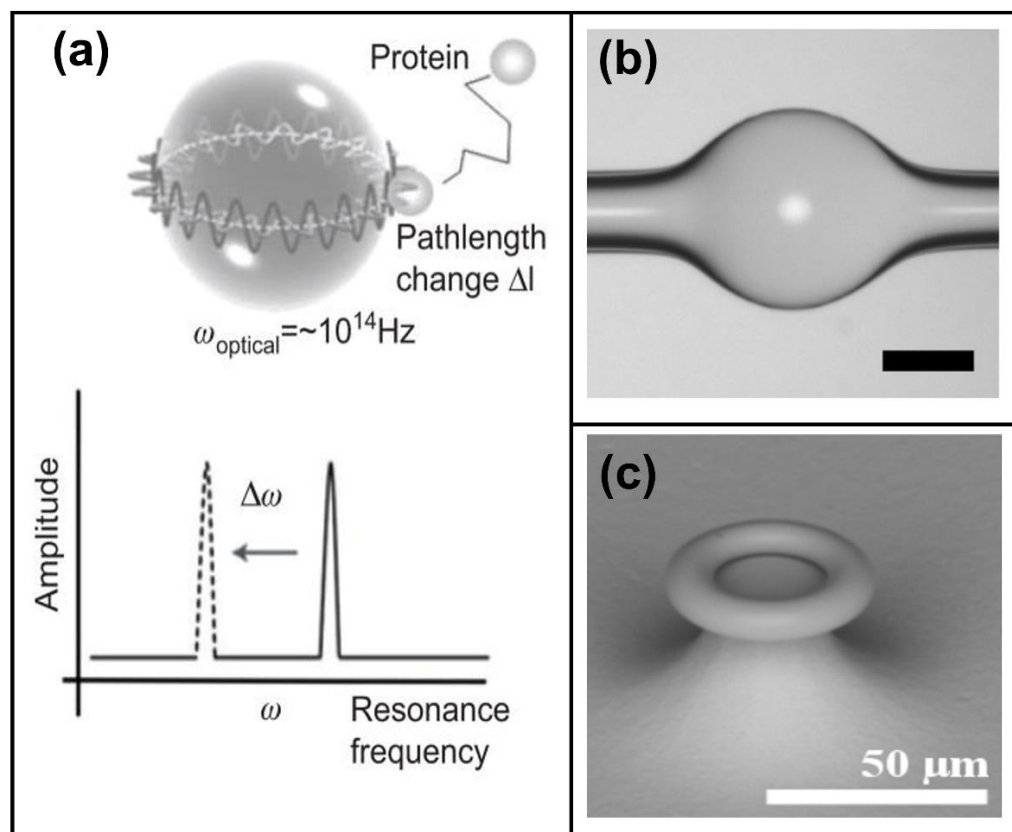

Figure 4. (**a**) Illustration of an optical resonance in a glass microsphere. The binding of a protein to the microsphere surface increases the whispering gallery mode (WGM) path length by Δl, producing a resonance frequency shift $\Delta \omega$. (**b**) Optical image of the microbubble resonator and (**c**) scanning electron micrograph (SEM) of as-fabricated microtoroid. (**a**) Reprinted with permission from [66], copyright 2012, De Gruyter. (**b**) Reprinted with permission from [75], copyright 2022, PNAS. (**c**) Reprinted with permission from [76], copyright 2010, MDPI.

All the geometries previously described can be configured alone, in a cascade [77] or in a series [78], and using an end-fire coupling, grating couplers, or a waveguide to couple the light into the resonant structure.

The advantages of using ring resonators for biological sensing include high sensitivity, multiplexed, label-free, and real-time detection, as well as low-cost and good integration and miniaturization capabilities thanks to the constant advances in standard CMOS fabrication techniques. However, the source coupling and readout integration into a smaller and simpler device remain a challenge, as well as the repeatability of the chip fabrications [79]. Even if efforts have been made to provide a portable system [79] or a complete packed LOC setup [80], only a few commercial solutions are currently available. Among the most notable commercial solutions is the Maverick® Diagnostic System (MDS) from Genalyte®, which uses silicon photonic ring resonators as the basis for their immunoassay analysis [65]. They can detect SARS-CoV-2 as well as 32 IgG and IgM antibody targets. With a small volume of blood in serum, it can deliver results in 20 min [81,82].

Due to the pandemic emergency announced by the World Health Organization (WHO) in 2020, several research teams have worked on a fast track to provide tools for label-free

and real-time detection of the SARS-CoV-2 virus, and photonic ring resonator systems provided a valuable resource [81,83]. For example, Cognetti et al. were able to monitor the spike proteins S1 and S2 of the SARS-CoV-2 using two ring resonators coupled in a series to a Si_3N_4 waveguide, obtaining promising results in the understanding of the molecular interactions of such proteins. Figure 5 depicts an example of LOC used for such studies [73].
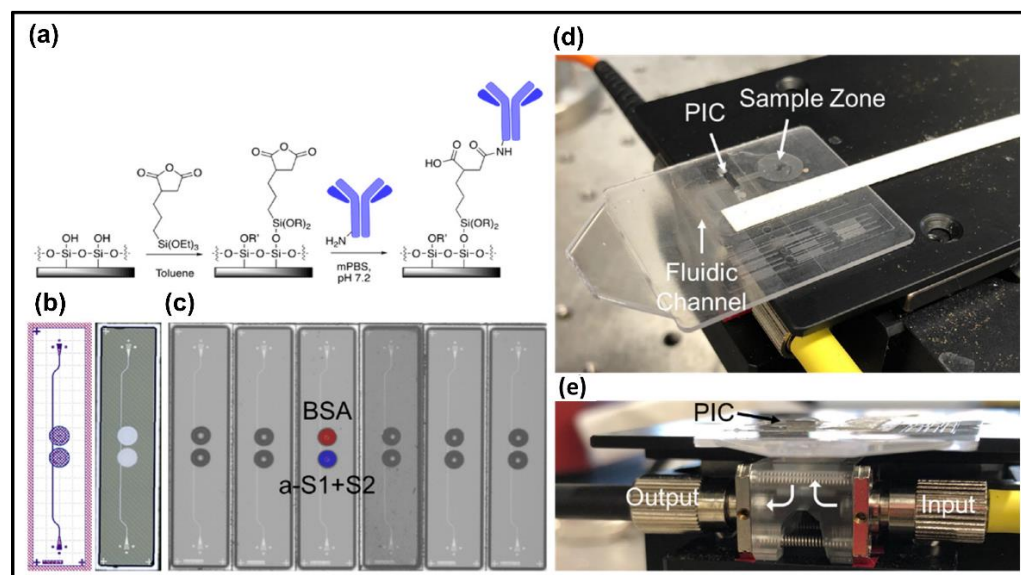

Figure 5. Disposable photonic assay platform. (**a**) Functionalization schematic. (**b**) GDS (graphic design system) and laser confocal image of the 1×4 mm photonic chips. (**c**) Image of antibody and antigen solutions spotted on chips with a Scienion SX microarrayer. (**d**) Image of the full microfluidic and photonic chip assembly. (**e**) Side view of the custom optical hub. Infrared light from a tunable laser is coupled vertically into and out of the photonic chip from below. Reprinted with permission from [73], copyright 2021, MDPI.

On the other hand, cancer detection has always been of main interest to society, and the advantages of ring resonator systems are remarkable [84]. Ali et al. proposed an optical ring resonator biosensor in 2020, including the theoretical analysis and simulations of the interactions with different types of carcinogenic cells [85].

Bacteria pathogens have also been studied for clinical, veterinary, and environmental purposes. For example, Figure 6 shows the LOC used for the detection of PCV2 viruses affecting swine livestock, which was achieved by Griol et al. obtaining limits of detection of 4.2 µg/mL by using two ring resonators coupled to a Si_3N_4 waveguide [86]. Another example is the detection of *E. coli* K12 in water using Si_3N_4 slot waveguide cascade ring resonators, obtaining a sensitivity of -80–461 nm/RIU and LOD of 1.33×10^{-5} by Sanati et al. [77].

Subramanian et al. showed, in 2021, the monitoring of single enzyme kinetics with a sub-ms time resolution using gold nanoparticles attached to a microsphere fabricated on the tip of a fiber optic [74].

Even single-strain DNA structures have been monitored and studied by employing ring resonators. In 2017, Jose Juan-Colas added an electrophotonic biosensor to a system of cascade racetracks resonators to study the conformational dynamics of DNA hairpins in real-time [87].

As part of future applications, microlasers directly built inside the cells are proposed for biosensing. This is a novel approach because there is no need to include bulky laser sources since the light source itself is built within the WGM resonator [88]. On the other hand, quantic sensing applications, as shown by Xavier et al., are under study [89]. In this case, instead of using the perturbance of the dipole moments of the light wave field due to the presence of single molecules, the author proposed to use the electric dipole

transitions between two electronic states and include the quantum effects. This way, it could be possible to detect a biomolecule or photon added or removed from the system, giving rise to quantum sensing.
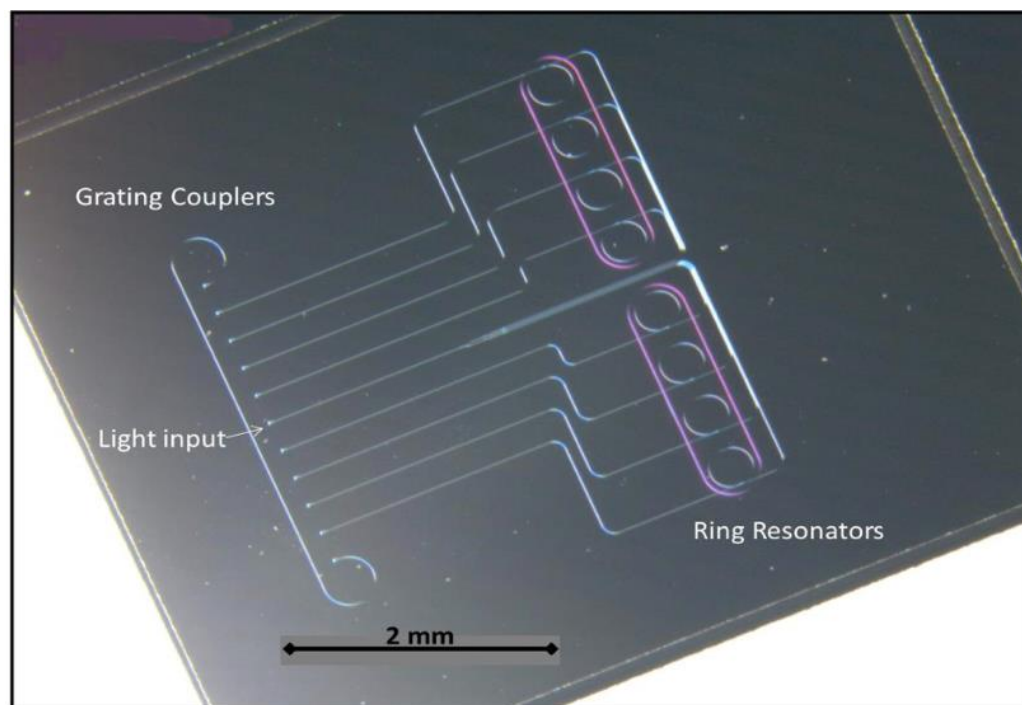

Figure 6. Fabricated PIC biosensor with ring resonators for the detection of PCV2 viruses on swine livestock. Reprinted with permission from [86], copyright 2019, MDPI.

2.3. Photonic Crystal Biosensors

Apart from the above-mentioned multiplexed optical biosensing methods, photonic crystals (PhCs) are an attractive technology for integration into biosensors devices. Currently, PhC devices have been employed for monitoring a variety of biomolecules, such as proteins, bacteria, cells, and nucleic acids, showing enormous potential in healthcare and precision medicine. PhCs consist of low-loss dielectric periodic dielectric materials in two or three directions that interact with light [90]. The logic behind this phenomenon was to facilitate an enhanced interaction between photons and the material medium in a controlled way, allowing the monitoring of food and water quality [91] and the identification of multiple molecules and bacteria in a single platform [92]. PhC is a material with its refractive index periodically modulated where the periodicity is expected to be comparable to the desired wavelength of light in the material [93]. This, in turn, makes it useful for sensing purposes due to the interaction of a target of interest with PhC changes in the local refractive index.

PhCs can be fabricated in many geometries, including slabs [94], microcavities [95], porous geometries [96], Bragg reflectors [97], and colloids [98] (see Figure 7). Photonic crystal nanostructures are fabricated using several techniques, including self-assembly methods and lithography. For instance, microparticles and colloids are transferred from a medium and self-assembled onto a surface via spin-coating or sedimentation to build a PhC structure with an iridescent color [99]. Regardless of the material surface, the standard process of fabrication is similar for almost all semiconductor photonic crystals. The patterns are primarily written using top-down approaches, including electron beam lithography (e-beam), electrochemical etching, nano-imprint lithography, and thin film deposition. The most common technique used for PhCs pattern exposure is e-beam, despite its relatively high cost and slow speed because of its versatility in the prototyping process (no masks required) [99]. Photolithography is a method that can be employed for pattern making.

In this process, the pattern is firstly defined using a photomask. UV light is shone on the surface, and the light interacts with the photoresist to create the desired patterns. The PhC patterns are transferred from the resist layer to the device surface using a dry chemical etches process such as reactive ion etching (RIE) or inductively coupled plasma (ICP). In some PhC sensor designs, the dry etch used to transfer the patterns to the material layer is followed by a wet etch to take off the layer underneath and leave the suspended layer.
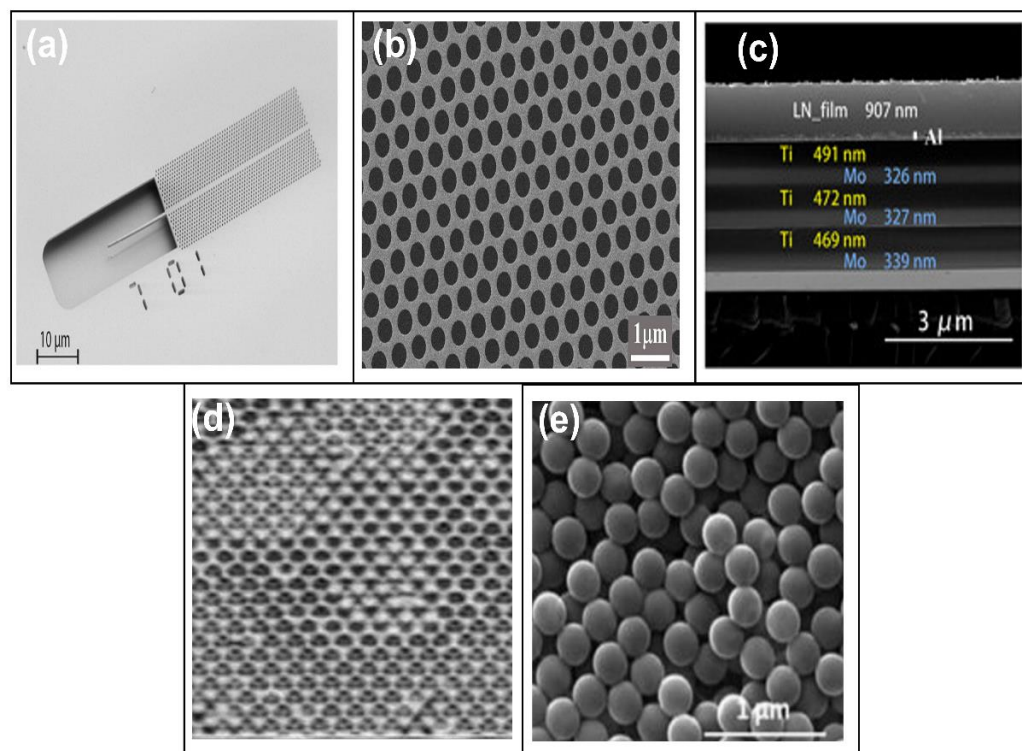

Figure 7. Photonic Crystals. (**a**) SEM image of a fabricated 2D PhC slab. (**b**) A representative SEM image of the nanohole PhC arrays (D = 350 nm). (**c**) Cross-sectional image of the LN thin film and the metallic multilayers (Bragg reflector). (**d**) Scanning electron micrographs of inverse opal I. (**e**) SEM of colloidal PhCs. (**a**) Reprinted with permission from [100], copyright 2019, Wiley; (**b**) reprinted with permission from [101], copyright 2022, Degruyter; (**c**) reprinted with permission from [102], copyright 2020, AIP; (**d**) reprinted with permission from [103], copyright 2009, IPS; (**e**) reprinted with permission from [104], copyright 2021, Elsevier.

In recent years, scientists have dedicated their knowledge to the development of POC platforms based on PhCs, and several devices have been developed. For example, Liu et al. proposed a POC using PhCs to detect urinary tract infections [105]. The biosensor chip comprised magnetic nanoparticles and luminescent ZGO: Mn NPs to be employed as an optical signal amplifier. As a result, limits of detection as low as 103 CFU/mL in human urine have been probed. Benelarbi et al. proposed a biosensor platform based on microcavities coupled to an optical waveguide and highlighted its sensitivity: around 97 nm/RIU and LOD of 0.0055 fg [106]. Biswas et al. [107] proposed a PhC-waveguide-based gas sensor for the monitoring of volatile organic compounds. The gas sensor comprised a micro-gas chromatography with a 2D PhC silicon slab. This gas sensor integration employed the advantages of an optical sensor, such as high sensitivity and rapid response time, and compensates for the lack of specificity that the label-free photonic sensors suffer. It has been demonstrated a fast separation and detection and a low limit of detection (ng).

With advances in nanofabrication, microfluidics, and smart materials, POC has seen tremendous advancements and promising portable platforms in biosensing applications. However, the integration of PhCs into a multiplexed platform is a challenge and limits the detection of several biomolecules in a single device. Here, we provide a broad perspective

using PhCs to detect multiple biomolecules in a single biosensing device using different structures. In recent years, 1D PhC configuration has been commonly used to develop a multi-target detection biosensor. One-dimensional configurations are structures with a high refractive index layer over a periodically arranged low refractive index grating layer, confining an electromagnetic field to the interface between the grating layer and the external medium under examination [108]. SiO_2, Ta_2O_5, and TiO_2 are typical materials used to fabricate 1D PhCs because they can combine label-free and fluorescence modes. Petrova et al. [109] (Figure 8) reported a real-time 1D PhC biosensor to monitor multiple ovarian cancer biomarkers, such as antigen 125, HER2, and antigen 15-3 in body-fluid samples. Three antibodies were immobilized onto the surface to create a capturing multiplexing array. The LOD estimated for HER2 was 0.62 pg/mL with linearity up to 50 pg/mL. A similar 1D PhC implementation was employed to monitor the Hepatitis B virus [110]. In particular, the antibody was used to detect surface antigen (HBsAg-ayw) and reached an LOD of 460 pg. This 1D-PhC biosensor was employed (Figure 8) as an imaging microarray platform (Like SPRi) and could interrogate hundreds of antigens. By using the same configuration, Rostova et al. [111] evaluated the binding kinetics of monoclonal antibodies to *E. coli*. (Figure 8). The bacteria were attached to PhC surfaces, and the interaction with the specific antibody was measured at concentrations ranging from 1.25 to 10 ug/mL.
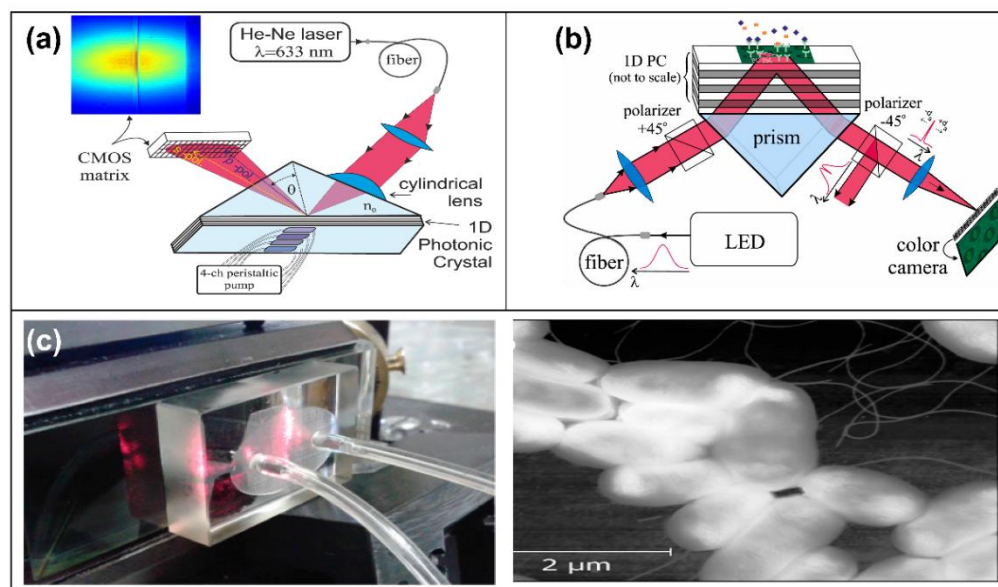

Figure 8. One-dimensional PhC biosensors: (**a**) Biosensor based on angle interrogation of a photonic crystal surface mode. (**b**) Schematic of the PhC SMi biosensor. Typical spectra of light as it passes from the LED to the color camera are shown. (**c**) A photograph of the flow cell and the photonic crystal behind it is attached to the prism via a refractive index matching oil and a topography atomic force microscopy (AFM) image of *E. coli* with flagella attached to the photonic crystal chip. (**a**) Reprinted with permission from [105], copyright 2019, Nature; (**b**) reprinted with permission from [109], copyright 2020, Elsevier; (**c**) reprinted with permission from [111], copyright 2016, MDPI.

Other classes of PhCs are those based on 2D and 3D structures, which can be designed using different types of symmetries. These sensors are notable for their small size, extraordinary sensitivity, and compatibility with standard microelectronic fabrication [112]. Zhou et al. designed single-slot photonic crystal nanobeam cavities on a silicon platform (Figure 9a). This design has demonstrated a high sensitivity of 244/RIU, which will be a promising candidate for future biosensor applications [113]. Yan et al. employed silicon bandpass filters for the multiplexing of high-sensitivity PhC microcavity biosensors (Figure 9b). This concept was demonstrated with a 2-channel microcavity PhC array containing PhC waveguide filters [114]. However, bio-applications with biofluids would be a big challenge for this technology. The last improvements in micro- and nanofabrica-

tion have allowed the designing of 3D-PhC configurations for optical biosensing. The most common 3D structures employed for biosensing are colloidal suspension of silica (SiO_2), polystyrene nano- and microspheres, or polymethyl-methacrylate spheres. Zhao and colleagues reported a biosensing methodology to detect bladder cancer using PhC barcodes as a transducer. These microspheres were functionalized with miRNA as probes to monitor multiple miRNA associated with bladder cancer. This methodology had an LOD of 1 nM in real fluids (Figure 9c) [115]. The Zhao group [116] recently reported the integration of a microneedle array with PhC barcodes which could be inserted into the skin and employed for the non-invasive detection of multiple biomarkers in skin fluids (Figure 9d). Gao et al. reported one of the most promising biosensors using PhCs, where a flexible, freestanding paper with a micropillar and nanocrystal was developed. This configuration could potentially develop multiplexing platforms and detect several cancer biomarkers [117].
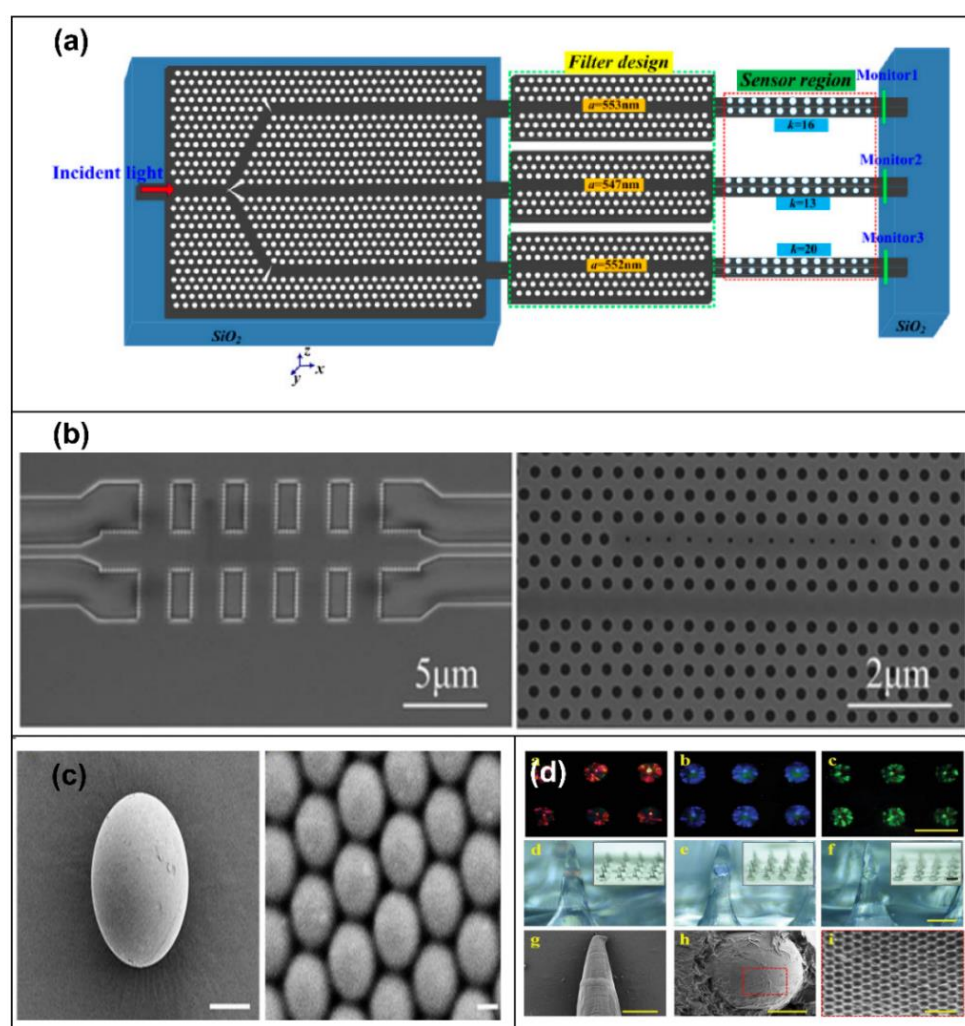

Figure 9. Two- and three-dimensional PhCs: (**a**) Schematic of the PhC's parallel integrated sensor array on the monolithic substrate. (**b**) Scanning electron microscope images of the waveguide crossings and PhCs microcavities. (**c**) SEM image of the surface of the PhC microsphere and the ordered hexagonal arrangement of monodisperse silica nanoparticles. (**d**) Optical and SEM images of the one-barcode-loaded microneedle array. (**a**) Reprinted with permission from [113], copyright 2016, MDPI. (**b**) Reprinted with permission from [114], copyright 2016, SPIE. (**c**) Reprinted with permission from [115], copyright 2020, the American Chemical Society. (**d**) Reprinted with permission from [116], copyright 2019, Wiley.

3. Plasmonic-Based Biosensors

Surface plasmon resonance (SPR) is electron oscillations that occur at the interface between two materials, one with positive permittivity and the other with negative permittivity, thanks to the presence of an electric field generated by an incident light beam [118]. This physical phenomenon has been implemented since the 1960s, and although its implementation in biosensors was reported for the first time in the 1980s [119], it was not until the 1990s that this type of transducer was popularization, generating several works where theoretical analyzes and experimental tests were demonstrated [120,121] with excellent academic and commercial results.

As previously said, the plasmonic resonances in a conductive surface are collective oscillations of electrons, which are the result of the induced interaction between the surface and an applied electric field. This type of system requires the incident light beam not to be perpendicular to the surface but to have an angle of incidence because according to the wavelength of the incident light beam, the thickness of the conductive layer, and the material that constitutes it. The specific angle at which the plasmonic resonance is observed can vary [122], as seen in Figure 10a,b. In addition, the specific resonance angle is affected by structural variations external to the conductive layer, for example, biological recognitions on its surface, which represent specific cases of biosensors based on SPRs.
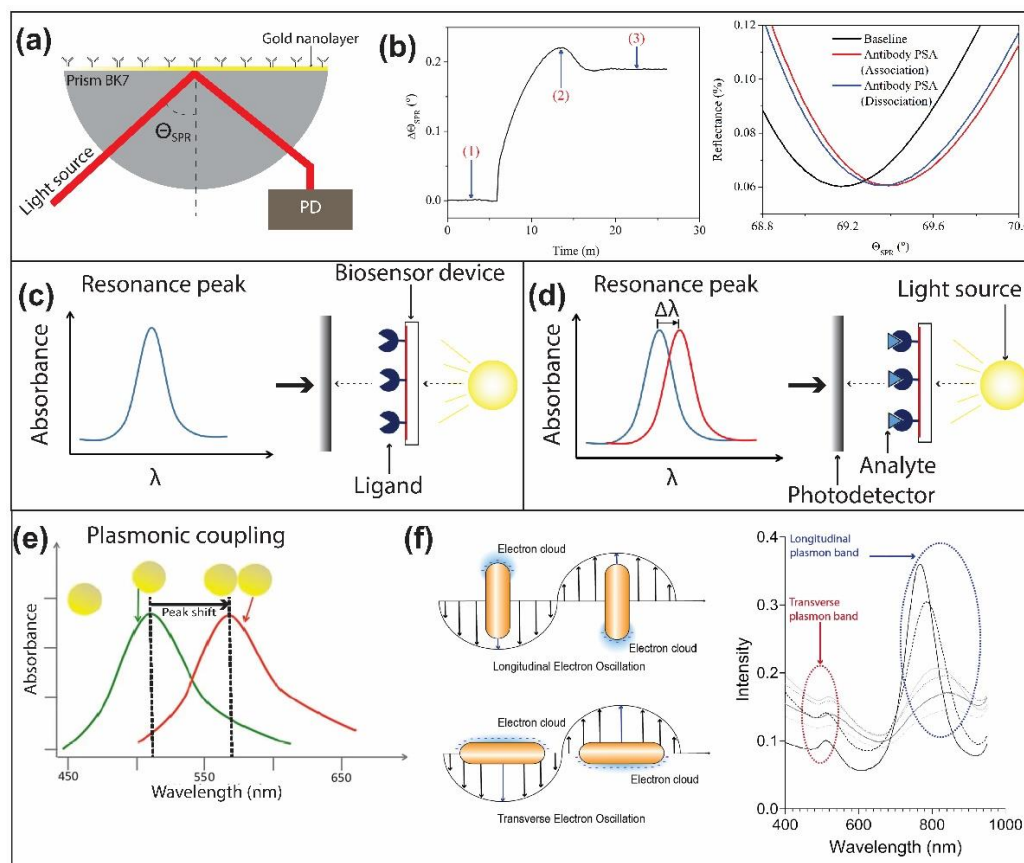

Figure 10. (**a**) Scheme of a traditional SPR system. (**b**) Behavioral description of the reflectance angle as a function of time and the Reflectance curve as a function of the variation baseline-antibody PSA (association)-antibody PSA (dissociation). The figures in (**c**,**d**) show the behavior of the resonance curve of a localized surface plasmon resonance (LSPR) system before and after achieving the biological recognition, respectively [123]. (**e**) Schematic demonstration of plasmonic coupling. (**f**) Resonance scheme in non-homogeneous nanoparticles, in this specific case, nanorods.

The implementation of metallic nanoparticles for the generation of localized surface plasmon resonances (LSPRs) [124] in bio-detection processes is a little more recent [125],

and thanks to this, it was possible to obtain multiple detections in a single measurement process as shown in [126,127]. In addition, a significant increase in the sensitivity of the devices was also observed, reaching sensitivities in the order of a few μg/mL.

Like the process described for biosensor devices based on the surface plasmon resonance, the principle of operation is based on the measurement of light absorption as a function of the variation of the wavelength of incident light. In this type of transducer, the size and distribution of the nanoparticles have a significant impact on the intensity and wavelength of absorption, as can be seen in Figure 10c,d. In Figure 10d, the wavelength of the absorption peak on the right side is red-shifted. This shift is quantified and reports the analyte's presence in a single sample. Equation (1) depicts the quantification of the peak shift,

$$\Delta\lambda \approx m(n_a - n_m)\left(1 - e^{(2d/l_d)}\right) \tag{1}$$

where m is a sensitivity factor in nm/RIU, n_a and n_m are the respective refractive indices of the biological layer, the aqueous medium d is the effective thickness of the biological layer, and l_d is the evanescent field decay length. It is important to keep in mind that by having multiple nanoparticles in an aqueous medium in constant interaction due to the electric field generated as a result of the incident light beam, it is necessary to keep all the nanoparticles together, guaranteeing plasmonic coupling between identical nanoparticles (Figure 10e), that is, all the nanoparticles behave as a single element, because the separation between them is less than the diameter of the nanoparticles used [128].

Multiple LSPR devices have been proposed to improve the performance of widely known and commercial SPR systems. However, most of the applications for disease detection in patient groups have been demonstrated in LSPR systems such as nanospheres [129] and nanorods [130], in which biochemical processes are developed, allowing serological differentiation of diseases such as dengue, zika, yellow fever virus (YFV), and Saint Louis encephalitis virus (SLEV), as demonstrated by [128,130], where it was also shown that detection processes with concentrations less than 4 μg/mL presented a greater error. This type of development, which has shown great potential, has led the scientific community to continue working on this technology, which has led to the development of devices with the most diverse configurations, considering materials, shapes, and distribution on the surface, aiming to get high-performance chips, which can be used to detect early-stage complex diseases.

LSPR devices have been regularly implemented in the form of nanospheres and nanorods, and when talking about devices fixed on surfaces in the form of nanodiscs [126] or nanocubes [123]. However, we have been able to observe more complex devices which use advanced manufacturing techniques, such as those demonstrated in suspended metal nanocylinders (685 nm/RIU) [131] or gold nanomushrooms (1010 nm/RIU) [132], which represent sensitivities three- and four-times higher than the sensitivities reached by conventional LSPR, respectively, that is, of the order of 200 nm/RIU approximately. All these attempts aim to increase the intensity of the resonant electric field in this type of device. In this sense, the work developed by Zhang et al. becomes highly relevant due to the theoretical and practical development, in which it is demonstrated how triangular nanoparticles or those in the form of crescent nanodiscs have a higher absorption peak intensity compared to nanocubes or filled nanodiscs, and all this, thanks to the angle formed in the vertices of the nanoparticle, demonstrates the importance of the vertices in nanoplasmonic devices, whose highest intensity was observed at a waist width of 70 nm (see Figure 11) [133].

All the previously mentioned developments and technologies are produced thanks to the research conducted in this area, and it suggests that performing multiplexed biosensing for the real-time, simultaneous detection of multiple diseases using LSPR would provide greater stability and precision in the biosensing processes compared to other technologies conceptually demonstrated so far [134,135]. In this sense, the experiences demonstrated to date are very few, but they provide excellent preliminary results. Chen et al. demonstrated, in 2015, nanoplasmonic microarrays based on nanorods fixed on the substrate. Through

microfluidic channels, it is possible to perform multiplexed analysis of cytokines from sampled human blood [136]. Similarly, it is possible to observe the detection of extracellular vesicles through imaging-based spectrometer-less optofluidic biosensors, which through well-defined microfluidic channels, simultaneously perform multiple detections [134].

In Figure 11, devices with configurations different from those previously mentioned can be observed. For example, there are integrated devices formed by plasmo-photoelectronic nanostructures [137] and devices based on a system of metallic nanoantennas with a gap of 3 nm, which allows them to obtain an electric field strong enough to reach a few-molecule detection range [138]. Other developments are devices in which metasurfaces based on dielectric nanometric structures integrable with CMOS are implemented, having plasmonic interaction as the operating principle [134,139]. This effect was first demonstrated in dielectric materials by Yavas et al. [135].
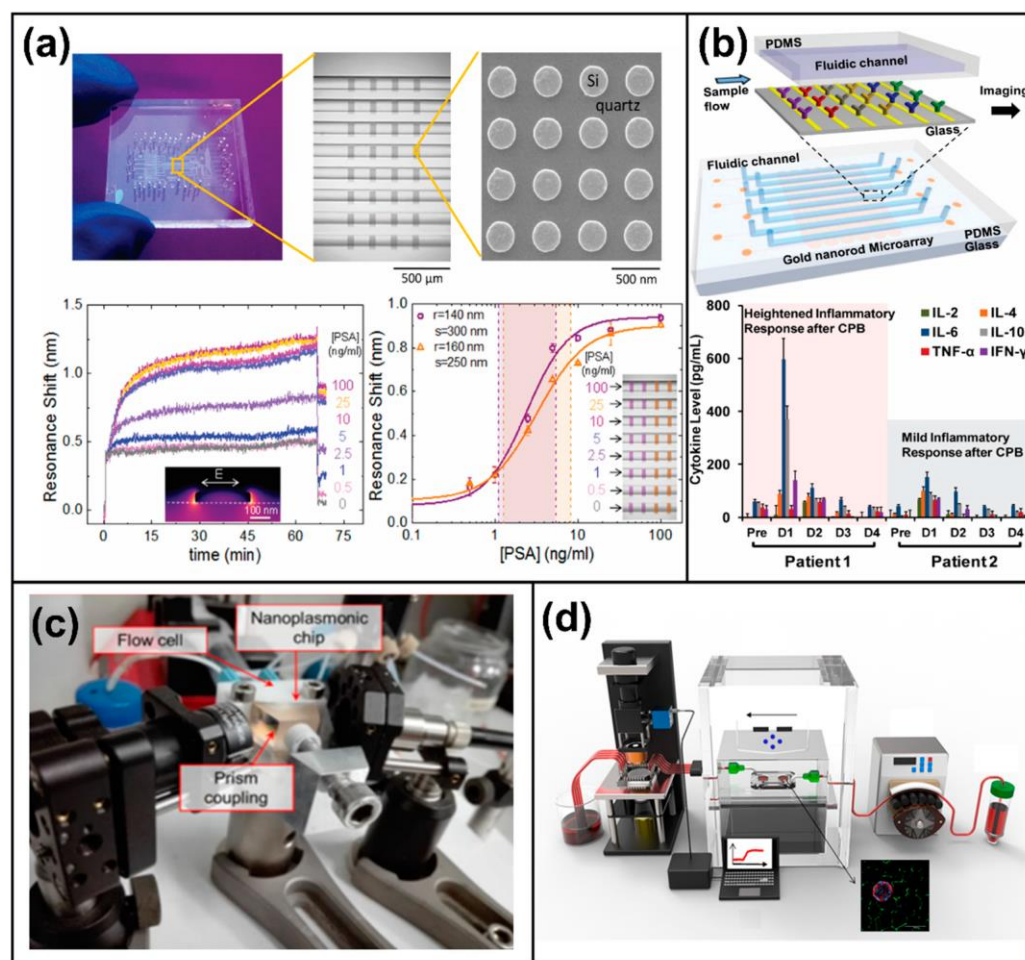

Figure 11. Examples of LSPR-based biosensors on-chip. (**a**) Multiplexed biosensor based on all-dielectric nanoresonator [135]. (**b**) Nanoplasmonic microarray for multiple and real-time detection of serum cytokine immunoassay [136]. (**c**) Photograph of the experimental LSPR setup [140]. (**d**) Schematic overview of the integration of the islet-on-a-chip (IOC) device with the on-chip LSPR sensing platform [141]. (**a**) Reprinted with permission from [135], copyright 2017, the American Chemical Society. (**b**) Reprinted with permission from [136], copyright 2015, the American Chemical Society. (**c**) Reprinted with permission from [140], copyright 2020, MDPI. (**d**) Reprinted with permission from [141], copyright 2021, MDPI.

Despite the excellent results obtained with on-chip LSPRs, it is necessary to improve developing manufacturing methods and ways of manipulating plasmonic effects to enhance its sensitivity. To date, most results observed in the literature continue to be proofs of concept where it is possible to appreciate an excellent performance as a biosensor, but

without the demonstration when analyzing specific diseases with real samples of human blood. This is one of the main challenges to be met by this type of device to consolidate itself as cutting-edge technology in biosensors.

4. Future Perspectives

It is remarkable the effort made by the scientific community to develop a multiplexed photonic biosensor. Devices with high sensitivity and excellent biochemical performance were enlisted. The development of complex systems based on sophisticated and novel manufacturing techniques and exploitation of physical phenomena to improve existing technologies were shown. It is expected that photonic biosensor platforms will become important, impacting the fields of clinical research, biodefense, drug discovery, healthcare, and food safety. However, a major weakness in the massification of photonic biosensors is the lack of clinical studies where the performance of these technologies is studied. This is mainly due to the complexity of in- and out-coupling systems; however, current technological developments provide the solution to these weaknesses. Furthermore, the design of bioreceptors that specifically match the analyte of interest and the design of universal functionalization surfaces with antifouling properties are crucial for developing photonic biosensors with high sensitivity and specificity.

Despite the benefits provided by LOC photonic biosensors, many challenges remain in the progression toward industrialization and commercialization of complete LOC platforms. Each disease and the conditions where the analysis and diagnosis take place will require the selection of the proper tool among the toolbox of LOCs previously shown. Considering constraints such as power availability, the reuse of the LOC cartridges, prices, reagents involved in the analysis, and so on, becomes a critical decision. Due to the interdisciplinary nature of the endeavor, the joint work of biotechnologists, chemists, electronics and photonics engineers, software developers, physicists, clean room technicians, medical doctors, physicians, and even patients is required. The correct orchestration of all the players involved and the planning of the technological development of the solutions become crucial as well.

Additionally, it should be noted that the emergence of highly infectious diseases such as SARS-CoV-2 has shown the importance of sensitive biosensors that allow diseases to be detected at an early stage and that are easy to manipulate; that is, it is essential to obtain POC systems that guarantee the real-time detection of multiple diseases simultaneously, through manipulation by end-users. This is a line of development that will be on the rise in the next few years.

The rise of wearables, the massive use of mobile smartphones, and the current hyperconnectivity will likely increase the demand for LOC systems. Smaller devices, seamlessly integrated into unimaginable places and devices as part of the rise of the Internet of things revolution, could become a reality. As shown, biosensors based on integrated photonics may have a key role in such technological evolution to unite the silica and the biological realms. In the distant future, it might even be possible to witness the birth and rise of quantic sensors, perhaps in quantic systems with quantic processors. Thus, several concepts relating to photonic biosensor platforms are being continuously applied. These can lead to the successful development of a highly sensitive, accurate, multiplexed, and fully integrated device for the diagnosis for a range of bioapplications.

References

1. Rodriguez-Mozaz, S.; Lopez de Alda, M.J.; Barceló, D. Biosensors as useful tools for environmental analysis and monitoring. *Anal. Bioanal. Chem.* **2006**, *386*, 1025–1041. [CrossRef] [PubMed]
2. Estevez, M.C.; Alvarez, M.; Lechuga, L.M. Integrated optical devices for lab-on-a-chip biosensing applications. *Laser Photonics Rev.* **2012**, *6*, 463–487. [CrossRef]
3. Rivet, C.; Lee, H.; Hirsch, A.; Hamilton, S.; Lu, H. Microfluidics for medical diagnostics and biosensors. *Chem. Eng. Sci.* **2011**, *66*, 1490–1507. [CrossRef]
4. Zamani, M.; Dupaty, J.; Baer, R.C.; Kuzmanovic, U.; Fan, A.; Grinstaff, M.W.; Galagan, J.E.; Klapperich, C.M. Paper-Based Progesterone Sensor Using an Allosteric Transcription Factor. *ACS Omega* **2022**, *7*, 5804–5808. [CrossRef]
5. Amín, N.; Torralba, A.S.; Álvarez-Diduk, R.; Afkhami, A.; Merkoçi, A. Lab in a Tube: Point-of-Care Detection of *Escherichia coli*. *Anal. Chem.* **2020**, *92*, 4209–4216. [CrossRef] [PubMed]
6. Temiz, Y.; Lovchik, R.D.; Kaigala, G.v.; Delamarche, E. Lab-on-a-chip devices: How to close and plug the lab? *Microelectron. Eng.* **2015**, *132*, 156–175. [CrossRef]
7. De la Paz, E.; Barfidokht, A.; Rios, S.; Brown, C.; Chao, E.; Wang, J. Extended Noninvasive Glucose Monitoring in the Interstitial Fluid Using an Epidermal Biosensing Patch. *Anal. Chem.* **2021**, *93*, 12767–12775. [CrossRef] [PubMed]
8. Cunningham, B.; Lin, B.; Qiu, J.; Li, P.; Pepper, J.; Hugh, B. A plastic colorimetric resonant optical biosensor for multiparallel detection of label-free biochemical interactions. *Sens. Actuators B Chem.* **2002**, *85*, 219–226. [CrossRef]
9. Qian, Y.; Zeng, X.; Gao, Y.; Li, H.; Kumar, S.; Gan, Q.; Cheng, X.; Bartoli, F.J. Intensity-modulated nanoplasmonic interferometric sensor for MMP-9 detection. *Lab Chip* **2019**, *19*, 1267–1276. [CrossRef]
10. Liu, Q.; Shin, Y.; Kee, J.S.; Kim, K.W.; Mohamed Rafei, S.R.; Perera, A.P.; Tu, X.; Lo, G.-Q.; Ricci, E.; Colombel, M.; et al. Mach–Zehnder interferometer (MZI) point-of-care system for rapid multiplexed detection of microRNAs in human urine specimens. *Biosens. Bioelectron.* **2015**, *71*, 365–372. [CrossRef]
11. Hsiao, Y.-P.; Mukundan, A.; Chen, W.-C.; Wu, M.-T.; Hsieh, S.-C.; Wang, H.-C. Design of a Lab-On-Chip for Cancer Cell Detection through Impedance and Photoelectrochemical Response Analysis. *Biosensors* **2022**, *12*, 405. [CrossRef] [PubMed]
12. Duval, D.; Osmond, J.; Dante, S.; Dominguez, C.; Lechuga, L.M. Grating couplers integrated on Mach-Zehnder interferometric biosensors operating in the visible range. *IEEE Photonics J.* **2013**, *5*, 3700108. [CrossRef]
13. Xu, D.-X.; Vachon, M.; Densmore, A.; Ma, R.; Delâge, A.; Janz, S.; Lapointe, J.; Li, Y.; Lopinski, G.; Zhang, D.; et al. Label-free biosensor array based on silicon-on-insulator ring resonators addressed using a WDM approach. *Opt. Lett.* **2010**, *35*, 2771–2773. [CrossRef] [PubMed]
14. Jahns, S.; Bräu, M.; Meyer, B.-O.; Karrock, T.; Gutekunst, S.B.; Blohm, L.; Selhuber-Unkel, C.; Buhmann, R.; Nazirizadeh, Y.; Gerken, M. Handheld imaging photonic crystal biosensor for multiplexed, label-free protein detection. *Biomed. Opt. Express* **2015**, *6*, 3724. [CrossRef]
15. Rosman, C.; Prasad, J.; Neiser, A.; Henkel, A.; Edgar, J.; Sönnichsen, C. Multiplexed Plasmon Sensor for Rapid Label-Free Analyte Detection. *Nano Lett.* **2013**, *13*, 3243–3247. [CrossRef]
16. Marn, A.M.; Needham, J.; Chiodi, E.; Ünlü, M.S. Multiplexed, high-sensitivity measurements of antibody affinity using interferometric reflectance imaging sensor. *Biosensors* **2021**, *11*, 483. [CrossRef]
17. Holgado, M.; Maigler, M.; Santamaría, B.; Hernandez, A.; Lavín, A.; Laguna, M.; Sanza, F.; Granados, D.; Casquel, R.; Portilla, J.; et al. Towards reliable optical label-free point-of-care (PoC) biosensing devices. *Sens. Actuators B Chem.* **2016**, *236*, 765–772. [CrossRef]
18. Murillo, A.M.M.; Tomé-Amat, J.; Ramírez, Y.; Garrido-Arandia, M.; Valle, L.G.; Hernández-Ramírez, G.; Tramarin, L.; Herreros, P.; Santamaría, B.; Díaz-Perales, A.; et al. Developing an Optical Interferometric Detection Method based biosensor for detecting specific SARS-CoV-2 immunoglobulins in Serum and Saliva, and their corresponding ELISA correlation. *Sens. Actuators B Chem.* **2021**, *345*, 130394. [CrossRef]
19. Shen, Y.; Huang, Z.; Huang, F.; He, Y.; Ye, Z.; Zhang, H.; Guo, C. A Self-Reference Interference Sensor Based on Coherence Multiplexing. *Front. Chem.* **2022**, *10*, 880081. [CrossRef]
20. Kozma, P.; Kehl, F.; Ehrentreich-Förster, E.; Stamm, C.; Bier, F.F. Integrated planar optical waveguide interferometer biosensors: A comparative review. *Biosens. Bioelectron.* **2014**, *58*, 287–307. [CrossRef]
21. Luan, E.; Shoman, H.; Ratner, D.M.; Cheung, K.C.; Chrostowski, L. Silicon photonic biosensors using label-free detection. *Sensors* **2018**, *18*, 3519. [CrossRef] [PubMed]
22. Gavela, A.F.; García, D.G.; Ramirez, J.C.; Lechuga, L.M. Last advances in silicon-based optical biosensors. *Sensors* **2016**, *16*, 285. [CrossRef] [PubMed]

23. Wang, J.; Sanchez, M.M.; Yin, Y.; Herzer, R.; Ma, L.; Schmidt, O.G. Silicon-Based Integrated Label-Free Optofluidic Biosensors: Latest Advances and Roadmap. *Adv. Mater. Technol.* **2020**, *5*, 1901138. [CrossRef]
24. Heideman, R.G.; Kooyman, R.P.H.; Greve, J. Development of an optical waveguide interferometric immunosensor. *Sens. Actuators B Chem.* **1991**, *4*, 297–299. [CrossRef]
25. Brandenburg, A.; Henninger, R. Integrated optical Young interferometer. *Appl. Opt.* **1994**, *33*, 5941. [CrossRef] [PubMed]
26. Brandenburg, A.; Krauter, R.; Künzel, C.; Stefan, M.; Schulte, H. Interferometric sensor for detection of surface-bound bioreactions. *Appl. Opt.* **2000**, *39*, 6396. [CrossRef]
27. Schipper, E.F.; Brugman, A.M.; Dominguez, C.; Lechuga, L.M.; Kooyman, R.P.H.; Greve, J. The realization of an integrated Mach-Zehnder waveguide immunosensor in silicon technology. *Sens. Actuators B Chem.* **1997**, *40*, 147–153. [CrossRef]
28. Lechuga, L.M.; Lenferink, A.T.M.; Kooyman, R.P.H.; Greve, J. Feasibility of evanescent wave interferometer immunosensors for pesticide detection: Chemical aspects. *Sens. Actuators B Chem.* **1995**, *25*, 762–765. [CrossRef]
29. Prieto, F.; Lveda, B.S.; Calle, A.; Llobera, A.; Nguez, C.D.; Abad, A.; Montoya, A.; Lechuga, L. An integrated optical interferometric nanodevice based on silicon technology for biosensor applications. *Nanotechnology* **2003**, *14*, 907–912. [CrossRef]
30. Densmore, A.; Vachon, M.; Xu, D.-X.; Janz, S.; Ma, R.; Li, Y.-H.; Lopinski, G.; Delâge, A.; Lapointe, J.; Luebbert, C.C.; et al. Silicon photonic wire biosensor array for multiplexed real-time and label-free molecular detection. *Opt. Lett.* **2009**, *34*, 3598–3600. [CrossRef]
31. Crespi, A.; Gu, Y.; Ngamsom, B.; Hoekstra, H.J.W.M.; Dongre, C.; Pollnau, M.; Ramponi, R.; van den Vlekkert, H.H.; Watts, P.; Cerulloa, G.; et al. Three-dimensional Mach-Zehnder interferometer in a microfluidic chip for spatially-resolved label-free detection. *Lab Chip* **2010**, *10*, 1167–1173. [CrossRef] [PubMed]
32. Yoshida, S.; Ishihara, S.; Arakawa, T.; Kokubun, Y. Highly sensitive optical biosensor based on silicon-microring-resonator-loaded Mach-Zehnder interferometer. *Jpn. J. Appl. Phys.* **2017**, *56*, 04CH08. [CrossRef]
33. Yadav, M.; Aksnes, A. Multiplexed Mach-Zehnder interferometer assisted ring resonator sensor. *Opt. Express* **2022**, *30*, 1388. [CrossRef] [PubMed]
34. Zhao, C.; Xu, L.; Liu, L. Ultrahigh sensitivity mach−zehnder interferometer sensor based on a weak one-dimensional field confinement silica waveguide. *Sensors* **2021**, *21*, 6600. [CrossRef]
35. Leuermann, J.; Fernández-Gavela, A.; Torres-Cubillo, A.; Postigo, S.; Sánchez-Postigo, A.; Lechuga, L.M.; Halir, R.; Molina-Fernández, Í. Optimizing the limit of detection of waveguide-based interferometric biosensor devices. *Sensors* **2019**, *19*, 3671. [CrossRef]
36. Dante, S.; Duval, D.; Sepúlveda, B.; González-Guerrero, A.B.; Sendra, J.R.; Lechuga, L.M. All-optical phase modulation for integrated interferometric biosensors. *Opt. Express* **2012**, *20*, 7195–7205. [CrossRef]
37. Halir, R.; Vivien, L.; le Roux, X.; Xu, D.-X.; Cheben, P. Direct and Sensitive Phase Readout for Integrated Waveguide Sensors. *IEEE Photonics J.* **2013**, *5*, 6800906. [CrossRef]
38. Molina-Fernández, Í.; Leuermann, J.; Ortega-Moñux, A.; Wangüemert-Pérez, J.G.; Halir, R. Fundamental limit of detection of photonic biosensors with coherent phase read-out. *Opt. Express* **2019**, *27*, 12616. [CrossRef]
39. Leuermann, J.; Stamenkovic, V.; Ramirez-Priego, P.; Sánchez-Postigo, A.; Fernández-Gavela, A.; Chapman, C.A.; Bailey, R.C.; Lechuga, L.M.; Perez-Inestrosa, E.; Collado, D.; et al. Coherent silicon photonic interferometric biosensor with an inexpensive laser source for sensitive label-free immunoassays. *Opt. Lett.* **2020**, *45*, 6595. [CrossRef]
40. Martens, D.; Ramirez-Priego, P.; Murib, M.S.; Elamin, A.A.; Gonzalez-Guerrero, A.B.; Stehr, M.; Jonas, F.; Anton, B.; Hlawatsch, N.; Soetaert, P.; et al. A low-cost integrated biosensing platform based on SiN nanophotonics for biomarker detection in urine. *Anal. Methods* **2018**, *10*, 3066–3073. [CrossRef]
41. Ramirez-Priego, P.; Martens, D.; Elamin, A.A.; Soetaert, P.; Van Roy, W.; Vos, R.; Anton, B.; Bockstaele, R.; Becker, H.; Singh, M.; et al. Label-Free and Real-Time Detection of Tuberculosis in Human Urine Samples Using a Nanophotonic Point-of-Care Platform. *ACS Sens.* **2018**, *3*, 2079–2086. [CrossRef] [PubMed]
42. Zinoviev, K.E.; Gonzalez-Guerrero, A.B.; Dominguez, C.; Lechuga, L.M. Integrated Bimodal Waveguide Interferometric Biosensor for Label-Free Analysis. *J. Light. Technol.* **2011**, *29*, 1926–1930. [CrossRef]
43. González-Guerrero, A.B.; Maldonado, J.; Dante, S.; Grajales, D.; Lechuga, L.M. Direct and label-free detection of the human growth hormone in urine by an ultrasensitive bimodal waveguide biosensor. *J. Biophotonics* **2017**, *10*, 61–67. [CrossRef] [PubMed]
44. Dante, S.; Duval, D.; Fariña, D.; González-Guerrero, A.B.; Lechuga, L.M. Linear readout of integrated interferometric biosensors using a periodic wavelength modulation. *Laser Photonics Rev.* **2015**, *9*, 248–255. [CrossRef]
45. Bassols-Cornudella, B.; Ramirez-Priego, P.; Soler, M.; Estevez, M.-C.; Luis-Ravelo, H.J.D.; Cardenosa-Rubio, M.; Lechuga, L.M. Novel Sensing Algorithm for Linear Read-Out of Bimodal Waveguide Interferometric Biosensors. *J. Light. Technol.* **2022**, *40*, 237–244. [CrossRef]
46. Liu, Q.; Kim, K.W.; Gu, Z.; Kee, J.S.; Park, M.K. Single-channel Mach-Zehnder interferometric biochemical sensor based on two-lateral-mode spiral waveguide. *Opt. Express* **2014**, *22*, 27910–27920. [CrossRef]
47. Ramirez, J.C.; Gabrielli, L.H.; Lechuga, L.M.; Hernandez-Figueroa, H.E. Trimodal waveguide demonstration and its implementation as a high order mode interferometer for sensing application. *Sensors* **2019**, *19*, 2821. [CrossRef]
48. Isayama, Y.H.; Hernández-Figueroa, H.E. High-order multimode waveguide interferometer for optical biosensing applications. *Sensors* **2021**, *21*, 3254. [CrossRef]

49. Torrijos-Morán, L.; Lisboa, B.D.; Soler, M.; Lechuga, L.M.; García-Rupérez, J. Integrated optical bimodal waveguide biosensors: Principles and applications. *Results Opt.* **2022**, *9*, 100285. [CrossRef]

50. Petrou, P.; Makarona, E.; Raptis, I.; Kakabakos, S.; Misiakos, K. Monolithically Integrated Label-Free Optical Immunosensors. *Eng. Proc.* **2022**, *16*, 11.

51. Vogelbacher, F.; Kothe, T.; Muellner, P.; Melnik, E.; Sagmeister, M.; Kraft, J.; Hainberger, R. Waveguide Mach-Zehnder biosensor with laser diode pumped integrated single-mode silicon nitride organic hybrid solid-state laser. *Biosens. Bioelectron.* **2022**, *197*, 113816. [CrossRef] [PubMed]

52. Angelopoulou, M.; Makarona, E.; Salapatas, A.; Misiakos, K.; Synolaki, E.; Ioannidis, A.; Chatzipanagiotou, S.; Ritvos, M.A.; Pasternack, A.; Ritvos, O.; et al. Directly immersible silicon photonic probes: Application to rapid SARS-CoV-2 serological testing. *Biosens. Bioelectron.* **2022**, *215*, 114570. [CrossRef]

53. Fernández-Gavela, A.; Herranz, S.; Chocarro, B.; Falke, F.; Schreuder, E.; Leeuwis, H.; Heideman, R.G.; Lechuga, L.M. Full integration of photonic nanoimmunosensors in portable platforms for on-line monitoring of ocean pollutants. *Sens. Actuators B Chem.* **2019**, *297*, 126758. [CrossRef]

54. Chalyan, T.; Potrich, C.; Schreuder, E.; Falke, F.; Pasquardini, L.; Pederzolli, C.; Heideman, R.; Pavesi, L. AFM1 detection in milk by fab' functionalized Si3N4 asymmetric mach-Zehnder interferometric biosensors. *Toxins* **2019**, *11*, 409. [CrossRef] [PubMed]

55. Chatzipetrou, M.; Gounaridis, L.; Tsekenis, G.; Dimadi, M.; Vestering-Stenger, R.; Schreuder, E.F.; Trilling, A.; Besselink, G.; Scheres, L.; van der Meer, A.; et al. A miniature bio-photonics companion diagnostics platform for reliable cancer treatment monitoring in blood fluids. *Sensors* **2021**, *21*, 2230. [CrossRef] [PubMed]

56. Besselink, G.; Schütz-Trilling, A.; Veerbeek, J.; Verbruggen, M.; van der Meer, A.; Schonenberg, R.; Dam, H.; Evers, K.; Lindhout, E.; Garritsen, A.; et al. Asymmetric Mach–Zehnder Interferometric Biosensing for Quantitative and Sensitive Multiplex Detection of Anti-SARS-CoV-2 Antibodies in Human Plasma. *Biosensors* **2022**, *12*, 553. [CrossRef]

57. Goodwin, M.J.; Besselink, G.A.J.; Falke, F.; Everhardt, A.S.; Cornelissen, J.J.L.M.; Huskens, J. Highly Sensitive Protein Detection by Asymmetric Mach-Zehnder Interferometry for Biosensing Applications. *ACS Appl. Bio. Mater.* **2020**, *3*, 4566–4572. [CrossRef]

58. Niu, H.; Yu, P.; Zhu, Y.; Jing, Z.; Li, P.; Wang, B.; Ma, C.; Wang, J.; Wu, J.; O Govorov, A.; et al. Mach-Zehnder interferometer based integrated-photonic acetone sensor approaching the sub-ppm level detection limit. *Opt. Express* **2022**, *30*, 29665–29679. [CrossRef]

59. Angelopoulou, M.; Petrou, P.; Misiakos, K.; Raptis, I.; Kakabakos, S. Simultaneous Detection of *Salmonella typhimurium* and *Escherichia coli* O157:H7 in Drinking Water and Milk with Mach–Zehnder Interferometers Monolithically Integrated on Silicon Chips. *Biosensors* **2022**, *12*, 507. [CrossRef]

60. Chocarro-Ruiz, B.; Herranz, S.; Fernandez-Gavela, A.; Sanchís, J.; Farre, M.; Marco, M.P.; Lechuga, L.M. Interferometric nanoimmunosensor for label-free and real-time monitoring of Irgarol 1051 in seawater. *Biosens. Bioelectron.* **2018**, *117*, 47–52. [CrossRef]

61. Ramirez-Priego, P.; Estévez, M.C.; Díaz-Luisravelo, H.J.; Manclús, J.J.; Montoya, Á.; Lechuga, L.M. Real-time monitoring of fenitrothion in water samples using a silicon nanophotonic biosensor. *Anal. Chim. Acta* **2021**, *1152*, 338276. [CrossRef] [PubMed]

62. Maldonado, J.; Estévez, M.C.; Fernández-Gavela, A.; González-López, J.J.; González-Guerrero, A.B.; Lechuga, L.M. Label-free detection of nosocomial bacteria using a nanophotonic interferometric biosensor. *Analyst* **2020**, *145*, 497–506. [CrossRef]

63. Maldonado, J.; González-Guerrero, A.B.; Domínguez, C.; Lechuga, L.M. Label-free bimodal waveguide immunosensor for rapid diagnosis of bacterial infections in cirrhotic patients. *Biosens. Bioelectron.* **2016**, *85*, 310–316. [CrossRef] [PubMed]

64. Huertas, C.S.; Fariña, D.; Lechuga, L.M. Direct and Label-Free Quantification of Micro-RNA-181a at Attomolar Level in Complex Media Using a Nanophotonic Biosensor. *ACS Sens.* **2016**, *1*, 748–756. [CrossRef]

65. Mudumba, S.; de Alba, S.; Romero, R.; Cherwien, C.; Wu, A.; Wang, J.; Gleeson, M.A.; Iqbal, M.; Burlingame, R.W. Photonic Ring Resonance Is a Versatile Platform for Performing Multiplex Immunoassays in Real Time. *J. Immunol. Methods* **2017**, *448*, 34–43. [CrossRef]

66. Vollmer, F.; Yang, L.; Fainman, S. Label-Free Detection with High-Q Microcavities: A Review of Biosensing Mechanisms for Integrated Devices. *Nanophotonics* **2012**, *1*, 267–291. [CrossRef]

67. Claes, T.; Molera, J.G.; de Vos, K.; Schacht, E.; Baets, R.; Bienstman, P. Label-Free Biosensing with a Slot-Waveguide-Based Ring Resonator in Silicon on Insulator. *IEEE Photonics J.* **2009**, *1*, 197–204. [CrossRef]

68. Voronin, K.; Stebunov, Y.; Voronov, A.A.; Arsenin, A.; Volkov, V.S. Vertically Coupled Plasmonic Racetrack Ring Resonator for Biosensor Applications. *Sensors* **2020**, *20*, 203. [CrossRef]

69. Flueckiger, J.; Schmidt, S.; Donzella, V.; Sherwali, A.; Ratner, D.M.; Chrostowski, L.; Cheung, K.C. Sub-Wavelength Grating for Enhanced Ring Resonator Biosensor. *Opt. Express* **2016**, *24*, 15672. [CrossRef]

70. Kwon, S.H. Plasmonicwaveguide Coupled Ring Cavity for a Non-Resonant Type Refractive Index Sensor. *Sensors* **2017**, *17*, 2526. [CrossRef]

71. Steglich, P.; Hülsemann, M.; Dietzel, B.; Mai, A. Optical Biosensors Based on Silicon-on-Insulator Ring Resonators: A Review. *Molecules* **2019**, *24*, 519. [CrossRef] [PubMed]

72. Perotto, S.; Biagini, C.; Hubarevich, A.; Tantussi, F.; de Angelis, F. Toward All on Chip Optical Detection in the Few Molecule Regime. *Biosens. Bioelectron.* **2020**, *169*, 112600. [CrossRef] [PubMed]

73. Cognetti, J.S.; Miller, B.L. Monitoring Serum Spike Protein with Disposable Photonic Biosensors Following SARS-CoV-2 Vaccination. *Sensors* **2021**, *21*, 5857. [CrossRef] [PubMed]

74. Subramanian, S.; Jones, H.B.L.; Frustaci, S.; Winter, S.; van der Kamp, M.W.; Arcus, V.L.; Pudney, C.R.; Vollmer, F. Sensing Enzyme Activation Heat Capacity at the Single-Molecule Level Using Gold-Nanorod-Based Optical Whispering Gallery Modes. *ACS Appl. Nano Mater.* **2021**, *4*, 4576–4583. [CrossRef] [PubMed]

75. Jin, L. Boost the sensitivity of optical sensors with interface modes. *Sci. Bull.* **2022**, *67*, 777–778.

76. Hunt, H.K.; Soteropulos, C.; Armani, A.M. Bioconjugation Strategies for Microtoroidal Optical Resonators. *Sensors* **2010**, *10*, 9317–9336. [CrossRef]

77. Sanati, P.; Hashemi, S.S.; Bahadoran, M.; Babadi, A.A.; Akbari, E. Detection of *Escherichia coli* K12 in Water Using Slot Waveguide in Cascaded Ring Resonator. *Silicon* **2022**, *14*, 851–857. [CrossRef]

78. Kasper, L.; Zein Al-Din, A.; Bruns, J.; Volkmer, R.; Petermann, K. Fix-Wavelength Multi-Analyte Detection with Serial SOI Ring Resonators. *Eng. Proc.* **2021**, *6*, 22.

79. Soni, V.; Chang, C.W.; Xu, X.; Wang, C.; Yan, H.; D Agati, M.; Tu, L.W.; Chen, Q.Y.; Tian, H.; Chen, R.T. Portable Automatic Microring Resonator System Using a Subwavelength Grating Metamaterial Waveguide for High-Sensitivity Real-Time Optical-Biosensing Applications. *IEEE Trans. Biomed. Eng.* **2021**, *68*, 1894–1902. [CrossRef]

80. Cognetti, J.S.; Steiner, D.J.; Abedin, M.; Bryan, M.R.; Shanahan, C.; Tokranova, N.; Young, E.; Klose, A.M.; Zavriyev, A.; Judy, N.; et al. Disposable Photonics for Cost-Effective Clinical Bioassays: Application to COVID-19 Antibody Testing. *Lab Chip* **2021**, *21*, 2913–2921. [CrossRef]

81. Iqbal, M.; Burlingame, R.W.; Romero, R.; Wang, A.; Grove, T.; Gleeson, M.A. Silicon Photonic Micro-Ring Resonators for Drug Screening and Kinetic Analysis. In *Label-Free Biosensor Methods in Drug Discovery*; Springer: New York, NY, USA, 2015; pp. 133–153.

82. Estrada, I.A.; Burlingame, R.W.; Wang, A.P.; Chawla, K.; Grove, T.; Wang, J.; Southern, S.O.; Iqbal, M.; Gunn, L.C.; Gleeson, M.A. Multiplex Detection of Pathogen Biomarkers in Human Blood, Serum, and Saliva Using Silicon Photonic Microring Resonators. In Proceedings of the Advances in Global Health through Sensing Technologies 2015, Baltimore, MD, USA, 13 May 2015; Volume 9490.

83. Toropov, N.; Osborne, E.; Joshi, L.T.; Davidson, J.; Morgan, C.; Page, J.; Pepperell, J.; Vollmer, F. SARS-CoV-2 Tests: Bridging the Gap between Laboratory Sensors and Clinical Applications. *ACS Sens.* **2021**, *6*, 2815–2837. [CrossRef] [PubMed]

84. Pongruengkiat, W.; Pechprasarn, S. Whispering-Gallery Mode Resonators for Detecting Cancer. *Sensors* **2017**, *17*, 2095. [CrossRef] [PubMed]

85. Ali, L.; Mohammed, M.U.; Khan, M.; Bin Yousuf, A.H.; Chowdhury, M.H. High-Quality Optical Ring Resonator-Based Biosensor for Cancer Detection. *IEEE Sens. J.* **2020**, *20*, 1867–1875. [CrossRef]

86. Griol, A.; Peransi, S.; Rodrigo, M.; Hurtado, J.; Bellieres, L.; Ivanova, T.; Zurita, D.; Sánchez, C.; Recuero, S.; Hernández, A.; et al. Design and Development of Photonic Biosensors for Swine Viral Diseases Detection. *Sensors* **2019**, *19*, 3985. [CrossRef]

87. Juan-Colás, J.; Krauss, T.F.; Johnson, S.D. Real-Time Analysis of Molecular Conformation Using Silicon Electrophotonic Biosensors. *ACS Photonics* **2017**, *4*, 2320–2326. [CrossRef]

88. Toropov, N.; Cabello, G.; Serrano, M.P.; Gutha, R.R.; Rafti, M.; Vollmer, F. Review of Biosensing with Whispering-Gallery Mode Lasers. *Light Sci. Appl.* **2021**, *10*, 42. [CrossRef]

89. Xavier, J.; Yu, D.; Vollmer, F.; Jones, C.; Zossimova, E. Quantum Nanophotonic and Nanoplasmonic Sensing: Towards Quantum Optical Bioscience Laboratories on Chip. *Nanophotonics* **2021**, *10*, 1387–1435. [CrossRef]

90. Xavier, J.; Vincent, S.; Meder, F.; Vollmer, F. Advances in optoplasmonic sensors—Combining optical nano/microcavities and photonic crystals with plasmonic nanostructures and nanoparticles. *Nanophotonics* **2018**, *7*, 1–38. [CrossRef]

91. Bonifacio, L.D.; Ozin, G.A.; Arsenault, A.C. Photonic Nose–Sensor Platform for Water and Food Quality Control. *Small* **2011**, *7*, 3153–3157. [CrossRef]

92. Bonifacio, L.D.; Puzzo, D.P.; Breslav, S.; Willey, B.M.; McGeer, A.; Ozin, G.A. Towards the Photonic Nose: A Novel Platform for Molecule and Bacteria Identification. *Adv. Mater.* **2010**, *22*, 1351–1354. [CrossRef]

93. Joannopoulos, J.D.; Johnson, S.G.; Winn, J.N.; Meade, R.D. Molding the Flow of Light. Princeton Univ. Press, Princeton, NJ [ua]. 2008. Available online: https://physics.mit.edu/wp-content/uploads/2021/01/physicsatmit_01_joannopolous.pdf (accessed on 23 September 2022).

94. Di Falco, A.; O'faolain, L.; Krauss, T. Chemical sensing in slotted photonic crystal heterostructure cavities. *Appl. Phys. Lett.* **2009**, *94*, 063503. [CrossRef]

95. Vahala, K.J. Optical microcavities. *Nature* **2003**, *424*, 839–846. [CrossRef]

96. Pacholski, C. Photonic crystal sensors based on porous Silicon. *Sensors* **2013**, *13*, 4694–4713. [CrossRef] [PubMed]

97. González-Pedro, V.; Calvo, M.E.; Míguez, H.; Maquieira, Á. Nanoparticle Bragg reflectors: A smart analytical tool for biosensing. *Biosens. Bioelectron. X* **2019**, *1*, 100012. [CrossRef]

98. Han, M.G.; Shin, C.G.; Jeon, S.J.; Shim, H.; Heo, C.J.; Jin, H.; Kim, J.W.; Lee, S. Full color tunable photonic crystal from crystalline colloidal arrays with an engineered photonic stop-band. *Adv. Mater.* **2012**, *24*, 6438–6444. [CrossRef]

99. Inan, H.; Poyraz, M.; Inci, F.; Lifson, M.A.; Baday, M.; Cunningham, B.T.; Demirci, U. Photonic crystals: Emerging biosensors and their promise for point-of-care applications. *Chem. Soc. Rev.* **2017**, *46*, 366–388. [CrossRef]

100. Li, M.; Liang, H.; Luo, R.; He, Y.; Lin, Q. High-Q 2D lithium niobate photonic crystal slab nanoresonators. *Laser Photonics Rev.* **2019**, *13*, 1800228. [CrossRef]

101. Zhang, Z.; Zhao, F.; Gao, R.; Jao, C.-Y.; Ma, C.; Li, J.; Li, X.; Guan, B.-O.; Cetin, A.E.; Chen, K. Rayleigh anomaly-enabled mode hybridization in gold nanohole arrays by scalable colloidal lithography for highly-sensitive biosensing. *Nanophotonics* **2022**, *11*, 507–517. [CrossRef]

102. Bai, X.; Shuai, Y.; Lv, L.; Huang, S.; Xing, Y.; Zhao, J.; Luo, W.; Wu, C.; Yang, T.; Zhang, W. Mo/Ti multilayer Bragg reflector for LiNbO3 film bulk acoustic wave resonators. *J. Appl. Phys.* **2020**, *128*, 094503. [CrossRef]

103. Grigoriev, S.; Napolskii, K.; Grigoryeva, N.; Vasilieva, A.; Mistonov, A.; Chernyshov, D.Y.; Petukhov, A.; Belov, D.; Eliseev, A.; Lukashin, A. Structural and magnetic properties of inverse opal photonic crystals studied by x-ray diffraction, scanning electron microscopy, and small-angle neutron scattering. *Phys. Rev. B* **2009**, *79*, 045123. [CrossRef]

104. Sansone, L.; Campopiano, S.; Pannico, M.; Giordano, M.; Musto, P.; Iadicicco, A. Photonic bandgap influence on the SERS effect in metal-dielectric colloidal crystals optical fiber probe. *Sens. Actuators B Chem.* **2021**, *345*, 130149. [CrossRef]

105. Liu, H.; Li, Z.; Shen, R.; Li, Z.; Yang, Y.; Yuan, Q. Point-of-care pathogen testing using photonic crystals and machine vision for diagnosis of urinary tract infections. *Nano Lett.* **2021**, *21*, 2854–2860. [CrossRef] [PubMed]

106. Benelarbi, D.; Bouchemat, T.; Bouchemat, M. Study of photonic crystal microcavities coupled with waveguide for biosensing applications. *Opt. Quantum Electron.* **2017**, *49*, 347. [CrossRef]

107. Biswas, P.; Zhang, C.; Chen, Y.; Liu, Z.; Vaziri, S.; Zhou, W.; Sun, Y. A portable micro-gas chromatography with integrated photonic crystal slab sensors on chip. *Biosensors* **2021**, *11*, 326. [CrossRef] [PubMed]

108. Shinn, M.; Robertson, W. Surface plasmon-like sensor based on surface electromagnetic waves in a photonic band-gap material. *Sens. Actuators B Chem.* **2005**, *105*, 360–364. [CrossRef]

109. Petrova, I.; Konopsky, V.; Nabiev, I.; Sukhanova, A. Label-Free Flow Multiplex Biosensing via Photonic Crystal Surface Mode Detection. *Sci. Rep.* **2019**, *9*, 8745. [CrossRef] [PubMed]

110. Konopsky, V.; Mitko, T.; Aldarov, K.; Alieva, E.; Basmanov, D.; Moskalets, A.; Matveeva, A.; Morozova, O.; Klinov, D. Photonic crystal surface mode imaging for multiplexed and high-throughput label-free biosensing. *Biosens. Bioelectron.* **2020**, *168*, 112575. [CrossRef]

111. Rostova, E.; Ben Adiba, C.; Dietler, G.; Sekatskii, S.K. Kinetics of antibody binding to membranes of living bacteria measured by a photonic crystal-based biosensor. *Biosensors* **2016**, *6*, 52. [CrossRef]

112. Baker, J.E.; Sriram, R.; Miller, B.L. Two-dimensional photonic crystals for sensitive microscale chemical and biochemical sensing. *Lab Chip* **2015**, *15*, 971–990. [CrossRef]

113. Zhou, J.; Huang, L.; Fu, Z.; Sun, F.; Tian, H. Multiplexed simultaneous high sensitivity sensors with high-order mode based on the integration of photonic crystal 1 × 3 beam splitter and three different single-slot PCNCs. *Sensors* **2016**, *16*, 1050. [CrossRef]

114. Yan, H.; Tang, N.; Jairo, G.A.; Chakravarty, S.; Blake, D.A.; Chen, R.T. High-sensitivity high-throughput chip based biosensor array for multiplexed detection of heavy metals. In Proceedings of the Frontiers in Biological Detection: From Nanosensors to Systems VIII, San Francisco, CA, USA, 13–18 February 2016; pp. 6–10.

115. Wei, X.; Bian, F.; Cai, X.; Wang, Y.; Cai, L.; Yang, J.; Zhu, Y.; Zhao, Y. Multiplexed detection strategy for bladder cancer microRNAs based on photonic crystal barcodes. *Anal. Chem.* **2020**, *92*, 6121–6127. [CrossRef] [PubMed]

116. Zhang, X.; Chen, G.; Bian, F.; Cai, L.; Zhao, Y. Encoded microneedle arrays for detection of skin interstitial fluid biomarkers. *Adv. Mater.* **2019**, *31*, 1902825. [CrossRef] [PubMed]

117. Gao, B.; Yang, Y.; Liao, J.; He, B.; Liu, H. Bioinspired multistructured paper microfluidics for POCT. *Lab Chip* **2019**, *19*, 3602–3608. [CrossRef]

118. Murray, W.A.; Barnes, W.L. Plasmonic materials. *Adv. Mater.* **2007**, *19*, 3771–3782. [CrossRef]

119. Liedberg, B.; Nylander, C.; Lunström, I. Surface plasmon resonance for gas detection and biosensing. *Sens. Actuators* **1983**, *4*, 299–304. [CrossRef]

120. Liedberg, B.; Nylander, C.; Lundström, I. Biosensing with surface plasmon resonance—How it all started. *Biosens. Bioelectron.* **1995**, *10*, i–ix. [CrossRef]

121. Leung, P.T.; Pollard-Knight, D.; Malan, G.P.; Finlan, M.F. Modelling of particle-enhanced sensitivity of the surface-plasmon-resonance biosensor. *Sens. Actuators B. Chem.* **1994**, *22*, 175–180. [CrossRef]

122. Ramirez, J.C.; Schianti, J.N.; Souto, D.E.P.; Kubota, L.T.; Hernandez-Figueroa, H.E.; Gabrielli, L.H. Dielectric barrier discharge plasma treatment of modified SU-8 for biosensing applications. *Biomed. Opt. Express* **2018**, *9*, 2168. [CrossRef]

123. Habib, A.; Zhu, X.; Can, U.I.; McLanahan, M.L.; Zorlutuna, P.; Yanik, A.A. Electro-plasmonic nanoantenna: A nonfluorescent optical probe for ultrasensitive label-free detection of electrophysiological signals. *Sci. Adv.* **2019**, *5*, eaav9786. [CrossRef]

124. Neuzil, P.; Reboud, J. Palm-Sized Biodetection System Based on Localized Surface Plasmon Resonance. *Anal. Chem.* **2008**, *80*, 6100–6103. [CrossRef]

125. Ruemmele, J.A.; Hall, W.P.; Ruvuna, L.K.; Van Duyne, R.P. A Localized Surface Plasmon Resonance Imaging Instrument for Multiplexed Biosensing. *Anal. Chem.* **2013**, *85*, 4560–4566. [CrossRef] [PubMed]

126. Demirdjian, B.; Bedu, F.; Ranguis, A.; Ozerov, I.; Henry, C.R. Water Adsorption by a Sensitive Calibrated Gold Plasmonic Nanosensor. *Langmuir* **2018**, *34*, 5381–5385. [CrossRef]

127. Klinghammer, S.; Uhlig, T.; Patrovsky, F.; Böhm, M.; Schütt, J.; Pütz, N.; Baraban, L.; Eng, L.M.; Cuniberti, G. Plasmonic Biosensor Based on Vertical Arrays of Gold Nanoantennas. *ACS Sens.* **2018**, *3*, 1392–1400. [CrossRef] [PubMed]

128. Machado, G.L.; Teixeira, F.M.F.; Ferreira, G.S.C.; Versiani, A.F.; Andrade, L.M.; Ladeira, L.O.; Fonseca, F.G.; Ramirez, J.C. Computational Guided Method Applied to LSPR-Based Biosensor for Specific Detection of the Four-Serotypes of Dengue Virus in Seropositive Patients. *Part. Part. Syst. Charact.* **2022**, *39*, 2100157. [CrossRef]

129. Behi, M.; Naficy, S.; Chandrawati, R.; Dehghani, F. Nanoassembled Peptide Biosensors for Rapid Detection of Matrilysin Cancer Biomarker. *Small* **2020**, *16*, 1905994. [CrossRef] [PubMed]

130. Versiani, A.F.; Martins, E.M.N.; Andrade, L.M.; Cox, L.; Pereira, G.C.; Barbosa-Stancioli, E.F.; Nogueira, M.L.; Ladeira, L.O.; da Fonseca, F.G. Nanosensors based on LSPR are able to serologically differentiate dengue from Zika infections. *Sci. Rep.* **2020**, *10*, 11302. [CrossRef]

131. Thilsted, A.H.; Pan, J.Y.; Wu, K.; Zór, K.; Rindzevicius, T.; Schmidt, M.S.; Boisen, A. Lithography-Free Fabrication of Silica Nanocylinders with Suspended Gold Nanorings for LSPR-Based Sensing. *Small* **2016**, *12*, 6745–6752. [CrossRef]

132. Shen, Y.; Zhou, J.; Liu, T.; Tao, Y.; Jiang, R.; Liu, M.; Xiao, G.; Zhu, J.; Zhou, Z.K.; Wang, X.; et al. Plasmonic gold mushroom arrays with refractive index sensing figures of merit approaching the theoretical limit. *Nat. Commun.* **2013**, *4*, 2381. [CrossRef]

133. Zhang, Z.; Zhou, B.; Huang, Y.; Liao, Z.; Li, Z.; Li, S.; Wang, S.; Wen, W. Gold crescent nanodisk array for nanoantenna-enhanced sensing in subwavelength areas. *Appl. Opt.* **2014**, *53*, 7236. [CrossRef]

134. Jahani, Y.; Arvelo, E.R.; Yesilkoy, F.; Koshelev, K.; Cianciaruso, C.; De Palma, M.; Kivshar, Y.; Altug, H. Imaging-based spectrometer-less optofluidic biosensors based on dielectric metasurfaces for detecting extracellular vesicles. *Nat. Commun.* **2021**, *12*, 4–13. [CrossRef]

135. Yavas, O.; Svedendahl, M.; Dobosz, P.; Sanz, V.; Quidant, R. On-a-chip Biosensing Based on All-Dielectric Nanoresonators. *Nano Lett.* **2017**, *17*, 4421–4426. [CrossRef] [PubMed]

136. Chen, P.; Chung, M.T.; McHugh, W.; Nidetz, R.; Li, Y.; Fu, J.; Cornell, T.T.; Shanley, T.P.; Kurabayashi, K. Multiplex serum cytokine immunoassay using nanoplasmonic biosensor microarrays. *ACS Nano* **2015**, *9*, 4173–4181. [CrossRef] [PubMed]

137. Park, Y.; Ryu, B.; Deng, Q.; Pan, B.; Song, Y.; Tian, Y.; Alam, H.B.; Li, Y.; Liang, X.; Kurabayashi, K. An Integrated Plasmo-Photoelectronic Nanostructure Biosensor Detects an Infection Biomarker Accompanying Cell Death in Neutrophils. *Small* **2020**, *16*, 1905611. [CrossRef] [PubMed]

138. Dong, L.; Yang, X.; Zhang, C.; Cerjan, B.; Zhou, L.; Tseng, M.L.; Zhang, Y.; Alabastri, A.; Nordlander, P.; Halas, N.J. Nanogapped Au Antennas for Ultrasensitive Surface-Enhanced Infrared Absorption Spectroscopy. *Nano Lett.* **2017**, *17*, 5768–5774. [CrossRef]

139. Yesilkoy, F.; Arvelo, E.R.; Jahani, Y.; Liu, M.; Tittl, A.; Cevher, V.; Kivshar, Y.; Altug, H. Ultrasensitive hyperspectral imaging and biodetection enabled by dielectric metasurfaces. *Nat. Photonics* **2019**, *13*, 390–396. [CrossRef]

140. Calvo-Lozano, O.; Aviñó, A.; Friaza, V.; Medina-Escuela, A.; SHuertas, C.; Calderón, E.J.; Eritja, R.; Lechuga, L.M. Fast and Accurate Pneumocystis Pneumonia Diagnosis in Human Samples Using a Label-Free Plasmonic Biosensor. *Nanomaterials* **2020**, *10*, 1246. [CrossRef]

141. Ortega, M.A.; Rodríguez-Comas, J.; Yavas, O.; Velasco-Mallorquí, F.; Balaguer-Trias, J.; Parra, V.; Novials, A.; Servitja, J.M.; Quidant, R.; Ramón-Azcón, J. In Situ LSPR Sensing of Secreted Insulin in Organ-on-Chip. *Biosensors* **2021**, *11*, 138. [CrossRef]